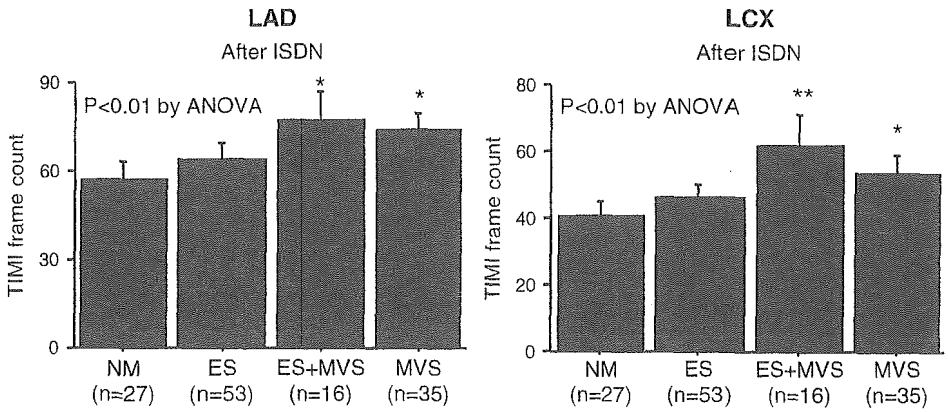

FIGURE 3. The effects of ISDN on TIMI frame count among the 4 groups. Intracoronary administration of ISDN did not improve the increased TIMI frame count in patients with both epicardial and microvascular spasm (ES+MVS) and MVS alone (MVS) (**$P < 0.01$ versus Normal or ES, *$P < 0.05$ versus Normal or ES).

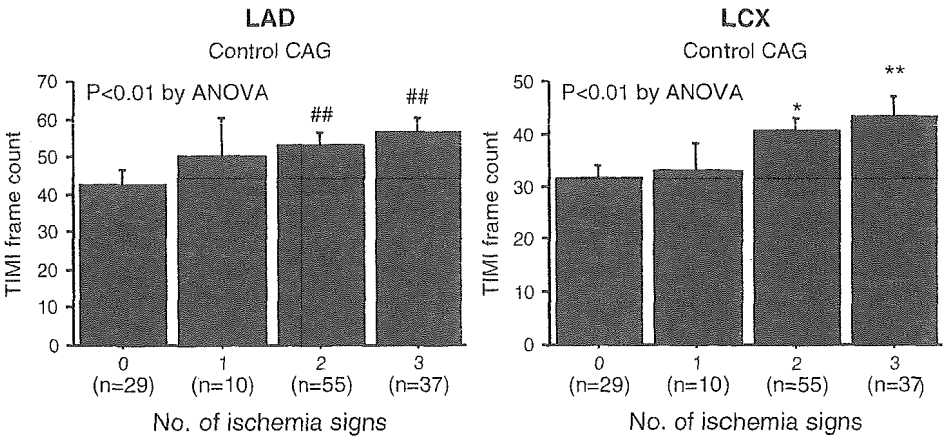

FIGURE 4. TIMI frame count in control coronary arteriograms (CAG) and CAG after ISDN in patients divided according to the number of ischemic signs. TIMI frame count was significantly increased in patients with more ischemic signs of chest pain, ischemic ECG changes, and myocardial lactate production, which was induced by 10 or 30 μg of intracoronary ACh under control conditions but not after intracoronary ISDN in both LAD and LCX (**$P < 0.01$ versus 0 or 1, *$P < 0.05$ versus 0 or 1, ##$P < 0.01$ versus 0, No., number).

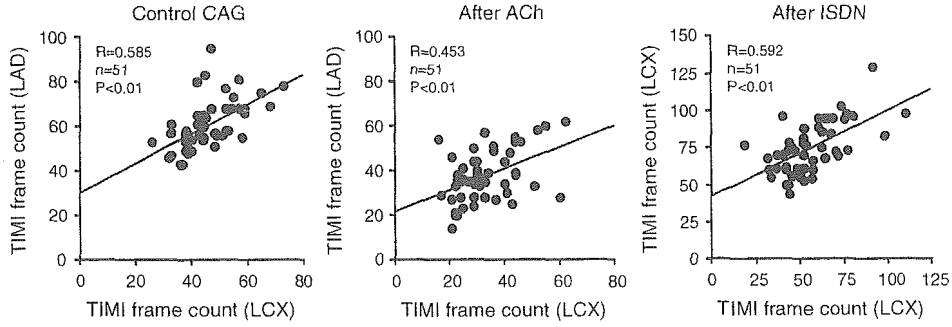

FIGURE 5. Correlations between LAD and LCX in TIMI frame count. TIMI frame count in LAD correlates well to that in LCX in patients with MVS, which suggested that impaired coronary microcirculation might exist in both LAD and LCX areas. CAG, coronary arteriograms.

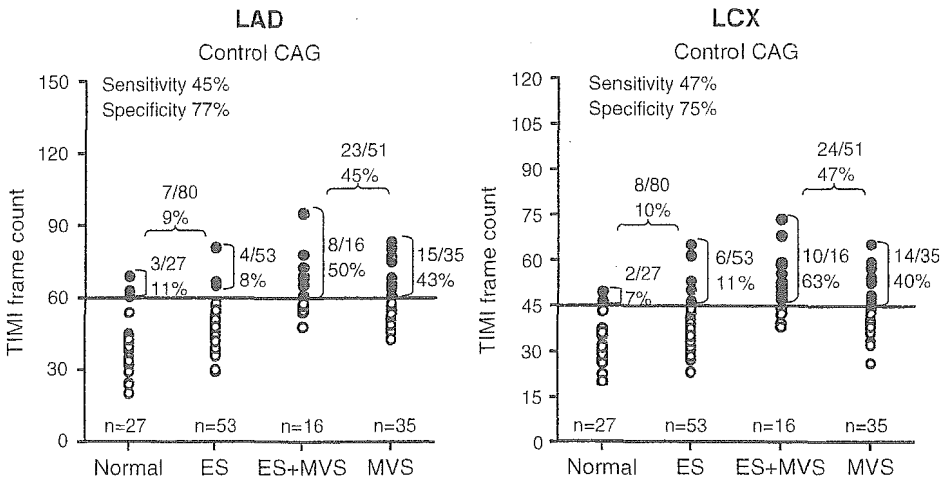

FIGURE 6. Usefulness in diagnosis of microvascular spasm. TIMI frame count of 60 or more in LAD showed a sensitivity of 45% and a specificity of 77% in control coronary arteriograms as a diagnosis of MVS. That of 45 or more in LCX showed a sensitivity of 47% and a specificity of 75%. CAG, coronary arteriograms.

frame count data with those on coronary flow reserve or endothelial function in patients with MVS. Third, because it is difficult to define the severity of microvascular angina, the new noninvasive technique or some marker is required to evaluate the severity of the microvascular circulation in the future. These points remain to be examined in a future study.

ACKNOWLEDGMENT

This study was supported in part by the Japan-China Sasagawa Medical Fellowship to H. Sun and by grants-in-aid (13307024, 15256003) of the Japanese Ministry of Education, Culture, Sports, Science and Technology, Tokyo, Japan.

REFERENCES

1. Mohri M, Koyanagi M, Egashira K, et al. Angina pectoris caused by coronary microvascular spasm. *Lancet.* 1998;351:1165–1169.
2. Masumoto A, Mohri M, Takeshita A. Three-year follow-up of the Japanese patients with microvascular angina attributable to coronary microvascular spasm. *Int J Cardiol.* 2001;81:151–156.
3. Ito A, Fukumoto Y, Shimokawa H. Changing characteristics of patients with vasospastic angina in the era of new calcium channel blockers. *J Cardiovasc Pharmacol.* 2004;44:480–485.
4. Clarke JG, Davies GJ, Kerwin R, et al. Coronary artery infusion of neuropeptide Y in patients with angina pectoris. *Lancet.* 1987;1:1057–1059.
5. Sun H, Mohri M, Shimokawa H, et al. Coronary microvascular spasm causes myocardial ischemia in patients with vasospastic angina. *J Am Coll Cardiol.* 2002;39:847–851.
6. Gibson CM, Cannon CP, Daley WL, et al. TIMI frame count: a quantitative method of assessing coronary artery flow. *Circulation.* 1996;93:879–888.
7. Kuga T, Egashira K, Inou T, et al. Correlation of basal coronary artery tone with constrictive response to ergonovine in patients with variant angina. *J Am Coll Cardiol.* 1993;22:144–150.
8. Bickel C, Rupprecht HJ, Maimaitiming A, et al. The superiority of TIMI frame count in detecting coronary flow changes after coronary stenting compared to TIMI Flow Classification. *J Invasive Cardiol.* 2002;14:590–596.
9. Mega JL, Morrow DA, Sabatine MS, et al. Correlation between the TIMI risk score and high-risk angiographic findings in non-ST-elevation acute coronary syndromes: observations from the Platelet Receptor Inhibition in Ischemic Syndrome Management in Patients Limited by Unstable Signs and Symptoms (PRISM-PLUS) trial. *Am Heart J.* 2005;149:846–850.
10. Kaski JC, Rosano GM, Collins P, et al. Cardiac syndrome X: clinical characteristics and left ventricular function. Long-term follow-up study. *J Am Coll Cardiol.* 1995;25:807–814.
11. Lanza GA, Colonna G, Pasceri V, et al. Atenolol versus amlodipine versus isosorbide-5-mononitrate on anginal symptoms in syndrome X. *Am J Cardiol.* 1999;84:854–856 A8.
12. Saitoh S, Onogi F, Aikawa K, et al. Multiple endothelial injury in epicardial coronary artery induces downstream microvascular spasm as well as remodeling partly via thromboxane A_2. *J Am Coll Cardiol.* 2001;37:308–315.
13. Metais C, Bianchi C, Li J, et al. Serotonin-induced human coronary microvascular contraction during acute myocardial ischemia is blocked by COX-2 inhibition. *Basic Res Cardiol.* 2001;96:59–67.
14. Shimokawa H. Cellular and molecular mechanisms of coronary artery spasm: lessons from animal models. *Jpn Circ J.* 2000;64:1–12.
15. Shimokawa H. Rho-kinase as a novel therapeutic target in treatment of cardiovascular diseases. *J Cardiovasc Pharmacol.* 2002;39:319–327.
16. Mohri M, Shimokawa H, Hirakawa Y, et al. Rho-kinase inhibition with intracoronary fasudil prevents myocardial ischemia in patients with coronary microvascular spasm. *J Am Coll Cardiol.* 2003;41:15–19.
17. Gibson CM, Murphy S, Menown IB, et al. Determinants of coronary blood flow after thrombolytic administration. TIMI Study Group. Thrombolysis in Myocardial Infarction. *J Am Coll Cardiol.* 1999;34:1403–1412.
18. Gibson CM, Cannon CP, Murphy SA, et al. Relationship of the TIMI myocardial perfusion grades, flow grades, frame count, and percutaneous coronary intervention to long-term outcomes after thrombolytic administration in acute myocardial infarction. *Circulation.* 2002;105:1909–1913.

Hypertension
Journal of the American Heart Association

Inhibition of Rho-Kinase in the Nucleus Tractus Solitarius Enhances Glutamate Sensitivity in Rats

Koji Ito, Yoshitaka Hirooka, Nobuaki Hori, Yoshikuni Kimura, Yoji Sagara, Hiroaki Shimokawa, Akira Takeshita and Kenji Sunagawa

Hypertension published online Jul 5, 2005;
DOI: 10.1161/01.HYP.0000177119.23178.05
Hypertension is published by the American Heart Association. 7272 Greenville Avenue, Dallas, TX 72514

 Print ISSN: 0194-911X. Online ISSN: 1524-4563

Inhibition of Rho-Kinase in the Nucleus Tractus Solitarius Enhances Glutamate Sensitivity in Rats

Koji Ito, Yoshitaka Hirooka, Nobuaki Hori, Yoshikuni Kimura, Yoji Sagara, Hiroaki Shimokawa, Akira Takeshita, Kenji Sunagawa

Abstract—The Rho/Rho–kinase pathway in the central nervous system is involved in the maintenance of dendritic spines, which form the postsynaptic contact sites of excitatory synapses. Inhibition of the Rho–kinase pathway in neuron promotes dendritic spines or branches. In contrast, activation of the Rho/Rho–kinase pathway reduces dendritic spines or branches. Recent studies suggest that morphological changes of dendritic spines occur rapidly, and spine morphology is associated with glutamate sensitivity. The aim of the present study was to determine whether Rho-kinase activity affects glutamate sensitivity in the nucleus tractus solitarii (NTS) of Wistar-Kyoto rats (WKY) and spontaneously hypertensive rats (SHR). We first examined the effects of unilateral glutamate injection in the NTS. There was a significantly smaller decrease in arterial pressure in SHR than in WKY. We then examined the depressor responses evoked by unilateral glutamate injection into the NTS after preinjection of Y-27632, a specific Rho-kinase inhibitor. Preinjection of Y-27632 enhanced the glutamate response in both strains. However, the magnitude of the augmentation was significantly greater in SHR than in WKY. Furthermore, we recorded single-unit activity of NTS neurons from medulla brain slice preparations. *N*-methyl-D-aspartate (NMDA) or α-amino-3-hydroxy-5-methyl-4-isoxazolepropionate (AMPA) was applied iontophoretically to the recorded neurons, and neuronal activity was recorded before and after Y-27632 perfusion. Y-27632 perfusion increased the response to NMDA and AMPA. These results suggest that inhibition of Rho-kinase activity in the NTS enhances glutamate sensitivity in WKY and SHR and might improve impaired glutamate sensitivity in SHR. (***Hypertension.* 2005;46:1-7.**)

Key Words: blood pressure ■ autonomic nervous system ■ amino acid ■ rats, spontaneously hypertensive ■ central nervous system

The Rho/Rho–kinase pathway regulates myosin light chain phosphorylation and contributes to smooth muscle contraction.[1–3] Y-27632, a selective Rho-kinase inhibitor, reduces arterial pressure in rat models of hypertension,[4] and Rho-kinase activity is enhanced in hypertensive blood vessels.[5,6] Thus, the Rho/Rho–kinase pathway is involved in the peripheral mechanisms of hypertension. We reported previously that Rho-kinase is present in the brain stem and maintains arterial pressure via the sympathetic nervous system, and that activation of the Rho/Rho–kinase pathway in the brain stem might contribute to the central mechanisms of hypertension.[7,8] Furthermore, inhibition of Rho-kinase in the nucleus tractus solitarii (NTS) enhances baroreflex control of heart rate (HR) in Wistar-Kyoto rats (WKY) and spontaneously hypertensive rats (SHR), probably because of a cardiac sympathoinhibitory effect.[9]

The Rho/Rho–kinase pathway in the central nervous system is involved in the maintenance of dendritic spines.[10] Dendritic spines form the postsynaptic contact sites of excitatory synapses in the central nervous system.[11] Inhibition of the Rho-kinase pathway in neuron promotes dendritic spines or branches. In contrast, activation of the Rho/Rho–kinase pathway reduces dendritic spines or branches.[10,12] Recent studies suggest that morphological changes of dendritic spines occur rapidly,[13] and spine morphology is associated with glutamate sensitivity.[14] Furthermore, GTPase-activating protein p250GAP, which is highly expressed in the brain, coexists with RhoA in dendritic spines and is involved in *N*-methyl-D-aspartate (NMDA) glutamate receptor activity-dependent actin reorganization in dendritic spines.[15] Furthermore, Rho-kinase in the brain stem contributes to arterial blood pressure regulation and baroreflex function.[7–9] The physiological role of Rho-kinase in neurons has not been clarified; however, these findings led to the hypothesis that inhibition of the Rho/Rho–kinase pathway in the NTS affects synaptic transmission, particularly in the excitatory synapses, via an enhanced response to glutamate. Therefore, the aim of the present study was to determine whether the Rho/Rho–kinase pathway in the NTS affects glutamate sensitivity in the NTS. For this purpose, we examined depressor responses

Received January 6, 2005; first decision January 20, 2005; revision accepted June 6, 2005.

From the Departments of Cardiovascular Medicine (K.I., Y.H., Y.K., Y.S., H.S., A.T., K.S.) and Pharmacology (N.H.), Kyushu University Graduate School of Medical Sciences, Fukuoka, Japan.

Correspondence to Yoshitaka Hirooka, MD, PhD, FAHA, Department of Cardiovascular Medicine, Kyushu University Graduate School of Medical Sciences, 3-1-1 Maidashi, Higashi-ku, Fukuoka 812-8582, Japan. E-mail hyoshi@cardiol.med.kyushu-u.ac.jp

Hypertension is available at http://www.hypertensionaha.org DOI: 10.1161/01.HYP.0000174328.06691.e9

evoked by microinjection of glutamate with or without preinjection of Y-27632 into the NTS of rats. Furthermore, in medulla slice preparations, we recorded single-unit activity of NTS neurons evoked by extracellular iontophoretic application of NMDA or α-amino-3-hydroxy-5-methyl-4-isoxazolepropionate (AMPA) before and after Y-27632 perfusion.

Methods

This study was reviewed and approved by the committee on ethics of animal experiments, Kyushu University Graduate School of Medical Sciences, and was conducted according to the guidelines for animal experiments of Kyushu University. Male WKY or SHR (280 to 340 g; 16 to 20 weeks old) were used in the present study. Rats were obtained from an established colony at the Animal Research Institute of Kyushu University Faculty of Medicine (Fukuoka, Japan).

Microinjection Study

Animals were anesthetized with sodium pentobarbital (50 mg/kg IP; followed by 10 to 20 mg/kg per hour IV), and a catheter was inserted into the right femoral artery for measurement of arterial pressure and HR and into the femoral vein for infusion of pentobarbital. The anesthetized animals were artificially ventilated and placed in a stereotaxic frame. The dorsal surface of the medulla was exposed, and the microinjection sites were defined according to a rat brain atlas:[16] the coordinates for the NTS were 0.6 mm rostral and 0.6 mm lateral to the calamus scriptorius and 0.5 mm below the dorsal surface of the medulla, as described previously.[17] Microinjection was performed with a micropipette connected to a Hamilton microsyringe. We used 3 doses of glutamate (2 pmol, 20 pmol, and 200 pmol; 0.1, 1.0, and 10 mmol/L in 20 nL, injected over a 5-s period) and tested 1 or 2 doses of glutamate in each rat. To test 2 doses of glutamate in 1 rat, we microinjected the lower dose first. More than 30 minutes after the microinjection of lower dose of glutamate, we replaced the pipette using the same coordinates, and then the higher dose of glutamate was microinjected into the NTS. In a preliminary study, we observed a similar depressor response to glutamate microinjected into the NTS using 2 separate pipettes with equal doses of glutamate. Care was taken to maintain stable arterial blood pressure and HR during the experiment. In the Y-27632 coinjection study, we used a 2-barrel micropipette. One side of the pipette was filled with glutamate and the other side with Y-27632 (40 pmol; 0.5 mmol/L in 80 nL, injected over a 20-s period) or vehicle (artificial cerebrospinal fluid [a-CSF]; 80 nL, injected over a 20-s period). First, we microinjected only glutamate and waited ≥30 minutes as in the single-barrel pipette experiments, and then Y-27632 (or a-CSF) and glutamate were injected. Because the glutamate response was rapid and of short duration, we microinjected glutamate into the NTS unilaterally 60 s after the Y-27632 or a-CSF injection. In addition, to avoid the possibility of differences in the amount of drug spread, a microdialysis probe with an external injection line (MI-A-I-12-01; Eicom) connected to a syringe pump was placed unilaterally into the NTS. We confirmed previously that the dialysis probe was permeable to NMDA.[18] Therefore, NMDA (0.5 mmol/L; infusion speed 2 μL/min for 5 minutes) was infused through a microdialysis probe and Y-27632 (5 mmol/L; injection speed 0.02 μL/min for 5 minutes) was injected through the injection line with syringe pumps.[18] We selected the dose of NMDA or Y-27632 to produce an arterial pressure reduction of the same magnitude as that produced by 2.0 to 20 pmol glutamate microinjection or 0.5 mmol/L Y-27632 microinjection into the NTS.

Single-Unit Recordings of NTS Neurons

We performed single-unit recordings of NTS neurons as described previously.[19–21] Under ether anesthesia, the rat was killed by cervical dislocation, and the brain stem was rapidly removed and placed in cold Krebs–Ringer solution containing 126 mmol/L NaCl, 5 mmol/L KCl, 2.4 mmol/L $CaCl_2$, 1.3 mmol/L $MgSO_4$, 1.26 mmol/L KH_2PO_4, 26 mmol/L $NaHCO_3$, and 10 mmol/L D-glucose, saturated with 95% O_2 and 5% CO_2. A horizontal brain stem slice (400-μm thick) containing the area postrema and NTS was obtained using a vibratome (DTK-1000; Dosaka). The slice was incubated for ≥2 hours in Krebs–Ringer solution bubbled with 95% O_2 and 5%CO_2 before starting the experiment. The recording chamber was perfused with oxygenated Krebs–Ringer solution at 34°C. Slices were placed on a Plexiglas mesh in a submerged recording chamber and covered with nylon mesh and a silver ring to support the tissue. The recording chamber was perfused with oxygenated Krebs–Ringer solution at a flow rate of 3 mL/min. Using a microscope, the NTS was visualized as a translucent area in the slice, and the electrode was advanced into the NTS until an action potential was recorded. The spikes were amplified (MWZ-7200 and MEG-1200; Nihon-Koden), and the raw neurogram and firing rate were displayed on an oscilloscope (DS-8605; Iwatsu) and recorded; the output was fed into a computer program Chart 4 (AD Instruments) to calculate the numbers of spikes per second. NMDA or AMPA was injected using a 2-barrel glass electrode, which was independent of the recording electrode. The most effective infusion field was a circular area ≈50 μm in diameter.[22] The iontophoretic system was a Neurophore model BH-2 control unit (Medical Systems), and the chemicals were prepared as follows: NMDA (50 mmol/L in distilled water, pH 7.5) and AMPA (10 mmol/L in 150 mmol/L NaCl, pH 7.5). The current used (1000-ms duration) was −5 to −30 nA for the NMDA pipette and −5 to −20 nA for the AMPA pipette. Retention current was not routinely applied. For NMDA and AMPA, the current was varied for each neuron because of the variations in electrodes and ejection sites, and then currents were adjusted to produce almost identical responses for NMDA and AMPA. The control firing rate in spikes per second (Hz) induced by NMDA or AMPA was recorded before and after Y-27632 perfusion. Y-27632 (50 μmol/L) was dissolved in oxygenated Krebs–Ringer solution and perfused at a flow rate of 3 mL/min for 6 minutes. The effects of Y-27632 were defined as the peak changes in spikes per second between before and after Y-27632 perfusion.

Statistical Analysis

All values are expressed as mean±SE. Two-way ANOVA was used to compare the responses of glutamate injection in each dose between WKY and SHR and the effects of Y-27632 on the responses to glutamate injection for each dose. Any 2 mean values were compared by application of the Bonferroni correction for multiple comparisons. Differences were considered to be statistically significant at a P value of <0.05.

Results

Baseline Characteristics

Baseline mean arterial pressure (MAP) and HR in each group are shown in the Table. MAP and HR were significantly higher in SHR than in WKY. Unilateral injection of Y-27632 induced a decrease in MAP and HR in SHR but not in WKY (Table).

Effects of Rho-Kinase Inhibition on Glutamate Sensitivity in the NTS

Unilateral microinjection of glutamate into the NTS decreased MAP in a dose-dependent manner in WKY and SHR (Figure 1). When lower doses of glutamate were microinjected, the magnitude of the decrease in MAP was significantly reduced in SHR compared with WKY (Figure 1). The percent change in MAP was significantly greater in WKY than in SHR for all doses of glutamate examined (Figure 1). The magnitude of the decrease in HR induced by glutamate injection did not differ between WKY and SHR (Figure 1). The magnitude of the MAP decrease evoked by unilateral glutamate injection after Y-27632 injection into the NTS was

Baseline MAP and HR Values (n=5 for each)

WKY-MAP					
Glu concentration	Control	After Glu	Control	After Y	After Glu
2.0 pmol	101±2	94±2	104±2	98±1	86±1
20 pmol	94±3	81±3	98±2	93±2	70±1
200 pmol	91±2	60±4	100±2	94±1	53±2
WKY-HR					
Glu concentration	Control	After Gill	Control	After Y	After Glu
2.0 pmol	309±7	304±6	304±7	301±6	292±7
20 pmol	301±6	294±6	295±7	291±8	274±10
200 pmol	299±8	276±9	305±7	300±8	269±10
SHR-MAP					
Glu concentration	Control	After Glu	Control	After Y	After Glu
2.0 pmol	163±2	159±2	163±2	146±4*	134±4
20 pmol	161±7	152±7	169±5	150±4†	122±4
200 pmol	167±3	141±4	166±3	151±6*	116±6
SHR-HR					
Glu concentration	Control	After Glu	Control	After Y	After Glu
2.0 pmol	320±4	314±3	325±3	308±6*	299±5
20 pmol	324±7	312±8	315±6	302±4*	279±4
200 pmol	313±4	276±6	317±5	295±7*	249±10

*$P<0.05$; †$P<0.01$ vs control.
Glu indicates glutamate; Y, Y-27632 (40 pmol;0.5 mmol/L in 80 nL).

significantly greater compared with glutamate injection alone in both strains (Figures 2 and 3). However, the magnitude of the augmentation was significantly greater in SHR than in WKY (glutamate dose 2 pmol: 1.8±0.2 versus 4.0±0.3; 20 pmol: 1.7±0.3 versus 3.1±0.3; 200 pmol: 1.2±0.1 versus 1.4±0.2; data are expressed as the relative ratio of the percent change compared with only glutamate injection, which was assigned a value of 1; $P<0.05$; n=5 for each). The magnitude of the HR decrease evoked by unilateral glutamate injection after Y-27632 injection into the NTS was significantly greater compared with only glutamate injection in both strains (Figures 2 and 3). Preinjection of a-CSF did not change the magnitude of the decrease in MAP induced by glutamate injection into the NTS (Figure 4A). The perfusion of NMDA unilaterally into the NTS through a dialysis probe decreased MAP, as reported previously.[18] The magnitude of the decrease in MAP induced by NMDA with Y-27632 injection was significantly greater than that by NMDA perfusion alone (Figure 4B).

Effects of Rho-Kinase Inhibition on Neuronal Activity in the NTS

Twelve neurons responded to iontophoretically applied NMDA and AMPA. Iontophoretic application of NMDA and AMPA transiently increased neuronal activity (Figure 5). Perfusion of Y-27632 increased neuronal activity evoked by NMDA and AMPA (NMDA 1.22±0.19 versus 1.78±0.19 spikes/s; $P<0.05$; AMPA 0.98±0.09 versus 1.33±0.11 spikes/s; n=12 for each; $P<0.05$).

Discussion

The present study demonstrated that inhibition of Rho-kinase activity in the NTS enhances glutamate sensitivity in WKY and SHR, and might improve the impaired glutamate sensitivity in SHR. The present observation might elucidate, at least in part, the mechanisms underlying differences in glutamate sensitivity in the NTS between WKY and SHR reported previously.[23] The glutamate concentration in the NTS is greater in SHR than in WKY.[24] These findings suggest that glutamate sensitivity in the NTS is decreased in SHR compared with WKY.

There is extensive literature regarding glutamate injections into the NTS of SHR and WKY.[25–27] Most of these studies report a similar depressor response to glutamate injected into the NTS between WKY and SHR. We reported a similar result in the previous study.[7] When we examined the dose response to glutamate injections in the present study; how-

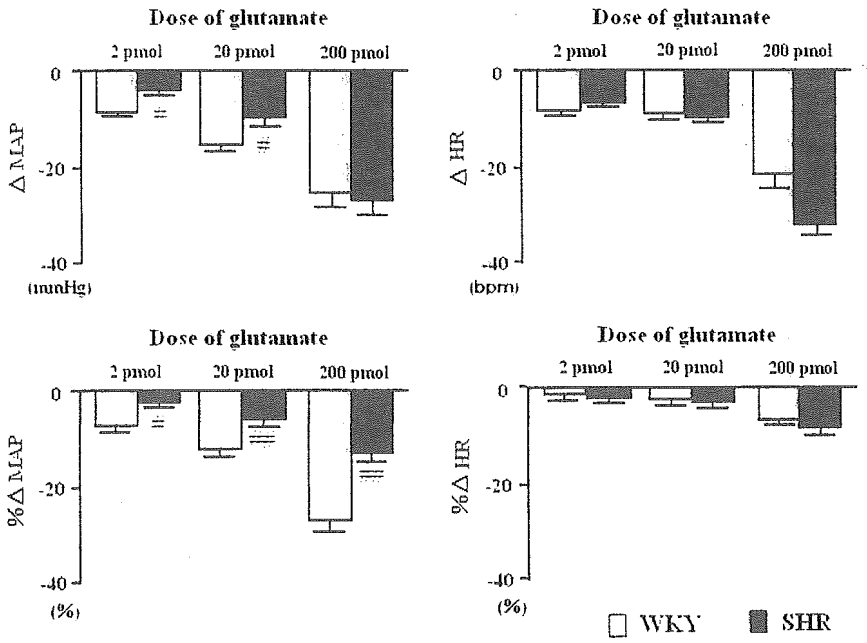

Figure 1. Effect of unilateral microinjection of glutamate into the NTS of WKY and SHR. Grouped data of responses evoked by unilateral injection of glutamate into the NTS (n=8 for each). #$P<0.05$; ##$P<0.01$ vs WKY.

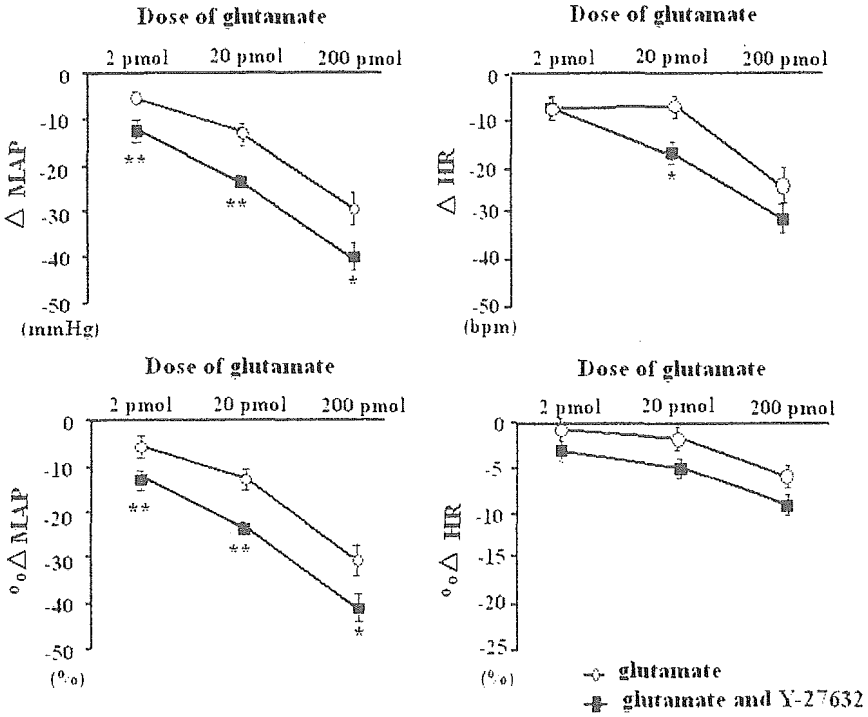

Figure 2. Effect of Rho-kinase inhibition on glutamate sensitivity in the NTS of WKY (n=5 for each). *$P<0.05$; **$P<0.01$ vs injection of only glutamate.

ever, there was less MAP reduction, particularly at lower doses, in SHR than in WKY. This result is consistent with that reported by Talman and Lewis.[23] However, it is difficult to compare the changes in MAP because there are baseline differences between the 2 groups. Talman and Lewis analyzed the data using repeated-measures ANOVA and covariate analysis to address the different MAP baseline values.[23] In the present study, we analyzed the data using a 2-way ANOVA with multiple comparison. Furthermore, we also compare the depressor response by percent change, as used previously.[28] In addition, there are structural vascular changes in SHR than in WKY.[29] Therefore, a greater depressor response is expected in SHR than in WKY. Nonetheless, a depressor response was demonstrated, suggesting an attenuated response to glutamate in SHR.

In the present study, we examined the effects of a Rho-kinase inhibitor on the decrease in arterial pressure evoked by unilateral glutamate injection into the NTS. The decrease in arterial pressure caused by glutamate injection after injection of Y-27632 was significantly greater than that by glutamate injec-

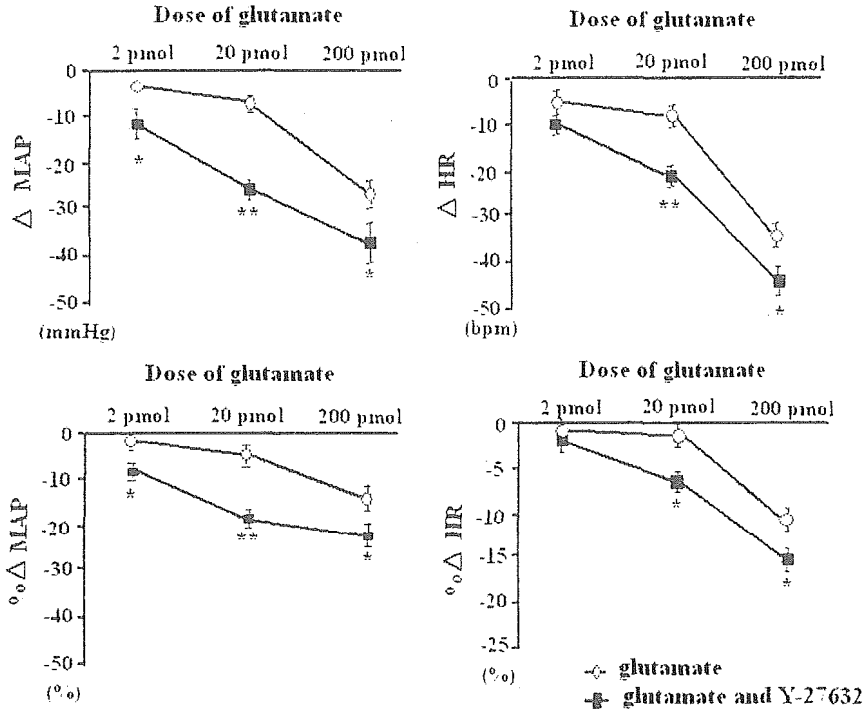

Figure 3. Effect of Rho-kinase inhibition on glutamate sensitivity in the NTS of SHR (n=5 for each). *$P<0.05$; **$P<0.01$ vs injection of only glutamate.

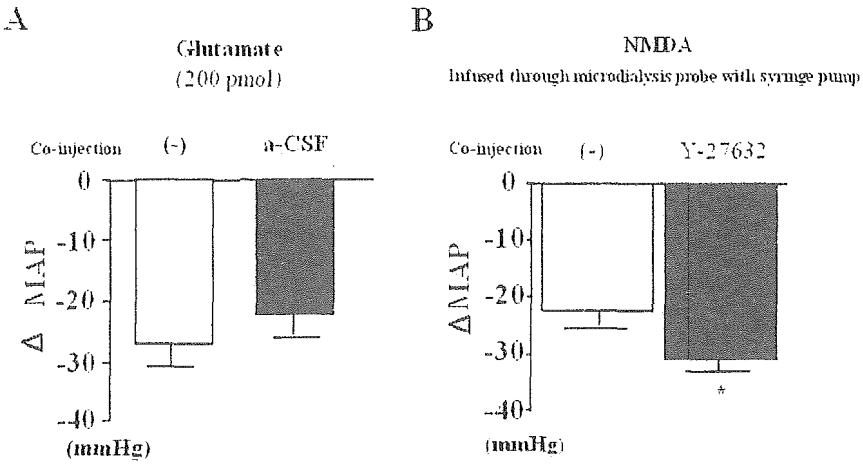

Figure 4. A, Effect of a-CSF on glutamate sensitivity in the NTS of WKY (n=3 for each). B, Effect of Rho-kinase inhibition on NMDA sensitivity in the NTS of WKY. NMDA and Y-27632 were applied using a microdialysis probe with a syringe pump (n=6 for each). *$P<0.05$ vs infusion of only NMDA.

tion alone in both strains. However, the magnitude of the augmentation was significantly greater in SHR than that in WKY, suggesting that inhibition of Rho-kinase in the NTS improves the impaired glutamate sensitivity in SHR. The HR responses to glutamate injection into the NTS did not differ between WKY and SHR (Figure 1), probably because this experiment was performed under anesthesia. However, the magnitude of HR reduction caused by glutamate was significantly augmented by preinjection of Y-27632 (Figures 2 and 3).

We took special care with the microinjection of glutamate to minimize differences in the amount of drug spread. However, differential drug spread is still possible, so we also used a microdialysis probe with an injection line that was connected to a syringe pump. Y-27632 was injected directly through the injection line, and NMDA was infused through the microdialysis probe, as described previously.[18] Infusion of only NMDA into the NTS decreased arterial pressure, as reported previously,[18] and infusion of NMDA with Y-27632 injection also decreased arterial pressure. However, the magnitude of the decrease in arterial pressure was significantly greater after infusion of NMDA with Y-27632 than that with NMDA alone. Therefore, the augmentation of the response to glutamate injection into the NTS is not likely to be attributable to differences in the amount of drug spread.

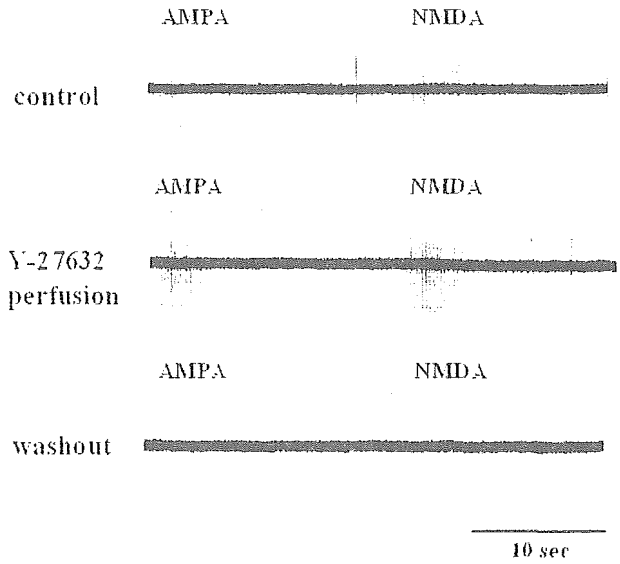

Figure 5. Effects of Y-27632 on neuronal activity in the NTS evoked by iontophoretically applied NMDA or AMPA. Example of raw neurograms indicating the increased neuronal activity after Y-27632 perfusion.

In the microinjection study, the effect of Rho-kinase inhibition on glutamate sensitivity was demonstrated indirectly. Therefore, we then recorded single-unit activity of NTS neurons to examine the direct effects of Rho-kinase inhibition. In the single-unit recording study, Rho-kinase inhibition increased the response of the recorded neurons to NMDA or AMPA. The magnitude of the augmentation differed in each recorded neuron. Because the NTS contains heterogenous neurons, including neurons related to cardiovascular control, it is possible that some of the recorded neurons did not contribute to baroreflex function, which might account for the different effects of Rho-kinase inhibition on the neurons.

We confirmed previously that the Rho/Rho–kinase pathway is activated in the NTS of SHR using Western blot analysis for membranous RhoA (translocation) or the phosphorylated ERM family (ezrin, radixin, moesin; target proteins of Rho-kinase).[7] These results suggest that activation of the Rho/Rho–kinase pathway is related to impaired glutamate sensitivity of the NTS neurons in SHR. As reported previously,[5] the Rho/Rho–kinase pathway plays an important role in regulating vascular tone. Therefore, it is possible that inhibition of Rho-kinase activity increases local blood flow and affects neuronal activity in the NTS. We consider it highly unlikely that the effects of Rho-kinase inhibition on arterial pressure regulation or neuronal activity in the NTS were caused by a local vasodilator effect because microinjection of another vasodilator, hydralazine, does not alter arterial pressure in either WKY or SHR.[7] In addition, the results using the brain slice preparation are independent from the vascular system.

In conclusion, inhibition of Rho-kinase in the NTS enhances glutamate sensitivity in the NTS. The Rho/Rho–kinase pathway in the NTS might be related to mechanism(s) underlying the resetting of baroreflex function in SHR via impaired glutamate sensitivity.

Perspectives

The precise mechanisms by which Rho-kinase inhibition in the NTS increases glutamate sensitivity cannot be elucidated

from the results of the present study. The small GTPase Rho and its downstream effector Rho-kinase are involved in many cellular functions.[30,31] The neuronal Rho/Rho–kinase pathway contributes to dendritic spine formation,[10] which forms the postsynaptic contact site for the majority of excitatory synapses.[11] Morphological changes in dendritic spines occur rapidly[13] and are associated with glutamate sensitivity.[14] Recently, it was demonstrated that there are structural differences in dendritic spines in the NTS between WKY and SHR.[32] However, that study also demonstrated that there were more GluR1-containig dendritic spines in the NTS of SHR compared with WKY, which was attributed to an increase in the proportion of dendritic spines containing GluR1 as well as an increase in the total number of dendritic spines.[32] Thus, it is unlikely that our observations are attributable to the morphological changes resulting from inhibition of the Rho/Rho–kinase pathway. Therefore, the effects of Rho-kinase inhibition might be produced not by the morphological changes in the dendritic spines (ie, an increase in the number of dendritic spines) but rather by a functional change in dendritic spines or other unknown mechanisms. Further studies are needed to clarify the mechanisms underlying our observations.

Acknowledgments

This study was supported by a grant-in-aid for scientific research (C13670721) from Japan Society for the Promotion of Science and by a grant for research on the autonomic nervous system and hypertension from Kimura Memorial Heart Foundation/Pfizer Pharmaceuticals, Inc.

References

1. Matsui T, Amano M, Yamamoto T, Chihara K, Nakafuku M, Ito M, Nakao T, Okawa K, Iwamatsu A, Kaibuchi K. Rho-associated kinase, a novel serine/threonine kinase, as a putative target for the small GTP binding protein Rho. *EMBO J.* 1996;15:2208–2216.
2. Laufs U, Liao JK. Targeting Rho in cardiovascular disease. *Circ Res.* 2000;87:526–528.
3. Kureishi Y, Kobayashi S, Amano M, Kimura K, Kanaide H, Nakano T, Kaibuchi K, Ito M. Rho-associated kinase directly induces smooth muscle contraction through myosin light chain phosphorylation. *J Biol Chem.* 1997;272:12257–12260.
4. Uehata M, Ishizaki T, Satoh H, Ono T, Kawahara T, Morishita, Tamakawa H, Yamagami K, Inui J, Maekawa M, Narumiya S. Calcium sensitization of smooth muscle mediated by a Rho-associated protein kinase in hypertension. *Nature.* 1997;389:990–994.
5. Mukai Y, Shimokawa H, Matoba T, Kandabashi T, Satoh S, Hiroki J, Kaibuchi K, Takeshita A. Involvement of Rho-kinase in hypertensive vascular disease: a novel therapeutic target in hypertension. *FASEB J.* 2001;15:1062–1064.
6. Masumoto A, Hirooka Y, Shimokawa H, Hironaga K, Setoguchi S, Takeshita A. Possible involvement of Rho-kinase in the pathogenesis of hypertension in humans. *Hypertension.* 2001;38:1307–1310.
7. Ito K, Hirooka Y, Sakai K, Kishi T, Kaibuchi K, Shimokawa H, Takeshita A. Rho/Rho-kinase pathway in brain stem contributes to blood pressure regulation via sympathetic nervous system: possible involvement in neural mechanisms of hypertension. *Circ Res.* 2003;92:1337–1343.
8. Ito K, Hirooka Y, Kishi T, Kimura Y, Kaibuchi K, Shimokawa H, Takeshita A. Rho/Rho-kinase pathway in the brainstem contributes to hypertension caused by chronic nitric oxide synthase inhibition. *Hypertension.* 2004;43:156–162.
9. Ito K, Hirooka Y, Sagara Y, Kimura Y, Kaibuchi K, Shimokawa H, Takeshita A, Sunagawa K. Inhibition of Rho-kinase in the brainstem augments baroreflex control of heart rate in rats. *Hypertension.* 2004;44:478–483.
10. Nakayama AY, Harms MB, Luo L. Small GTPases Rac and Rho in the maintenance of dendritic spines and branches in hippocampal pyramidal neurons. *J Neurosci.* 2000;20:5329–5338.
11. Koch C, Zador A. The function of dendritic spines: devices subserving biochemical rather than electrical compartmentalization. *J Neurosci.* 1993;13:413–422.
12. Bito H, Furuyashiki T, Ishihara H, Shibasaki Y, Ohashi K, Mizuno K, Maekawa M, Ishizaki T, Narumiya S. A critical role for a Rho-associated kinase, p160ROCK, in determining axon outgrowth in mammalian CNS neurons. *Neuron.* 2000;26:431–441.
13. Fischer M, Kaech S, Knutti D, Matus A. Rapid actin-based plasticity in dendritic spines. *Neuron.* 1998;20:847–854.
14. Matsuzaki M, Ellis-Davies GC, Nemoto T, Miyashita Y, Iino M, Kasai H. Dendritic spine geometry is critical for AMPA receptor expression in hippocampal CA1 pyramidal neurons. *Nat Neurosci.* 2001;4:1086–1092.
15. Nakazawa T, Watabe AM, Tezuka T, Yoshida Y, Yokoyama K, Umemori H, Inoue A, Okabe S, Manabe T, Yamamoto T. p250GAP, a novel brain-enriched GTPase-activating protein for Rho family GTPases, is involved in the *N*-methyl-D-aspartate receptor signaling. *Mol Biol Cell.* 2003;14:2921–2934.
16. Paxinos G, Watson C. *The Rat Brain in Stereotaxic Coordinates.* 4th ed. New York, NY: Academic Press; 1998.
17. Shigematsu H, Hirooka Y, Eshima K, Shihara M, Tagawa T, Takeshita A. Endogenous angiotensin II in the NTS contributes to sympathetic activation in rats with aortocaval shunt. *Am J Physiol.* 2001;280:R1665–R1673.
18. Matsuo I, Hirooka Y, Hironaga K, Eshima K, Shigematsu H, Shihara M, Sakai K, Takeshita A. Glutamate release via NO production evoked by NMDA in the NTS enhances hypotension and bradycardia in vivo. *Am J Physiol.* 2001;280:R1285–R1291.
19. Shihara M, Hirooka Y, Hori N, Matsuo I, Tagawa T, Suzuki S, Akaike N, Takeshita A. Endothelin-1 increases the neuronal activity and augments the responses to glutamate in the NTS. *Am J Physiol.* 1998;44:R658–R665.
20. Shihara M, Hori N, Hirooka Y, Eshima K, Akaike N, Takeshita A. Cholinergic systems in the nucleus of the solitary tract of rats. *Am J Physiol.* 1999;276:R1141–R1148.
21. Tagawa T, Imaizumi T, Harada S, Endo T, Shiramoto M, Hirooka Y, Takeshita A. Nitric oxide influences neuronal activity in the nucleus tractus solitarius of rat brainstem slices. *Circ Res.* 1994;75:70–76.
22. Hori N, Auker CR, Braitman DJ, Carpenter DO. Pharmacologic sensitivity of amino acid responses and synaptic activation of in vitro prepyriform neurons. *J Neurophysiol.* 1982;48:1289–1301.
23. Talman WT, Lewis SJ. Altered cardiovascular responses to glutamate and acetylcholine microinjected into the nucleus tractus solitarii of the SHR. *Clin Exp Hypertens.* 1991;13:661–668.
24. Kubo T, Kihara M, Misu Y. Altered amino acid levels in brainstem regions of spontaneously hypertensive rats. *Clin Exp Hypertens.* 1996;11:233–241.
25. Katsunuma N, Tsukamoto K, Ito S, Kanmatsuse K. Enhanced angiotensin-mediated responses in the nucleus tractus solitarii of spontaneously hypertensive rats. *Brain Res Bull.* 2003;60:209–214.
26. Matsumura K, Averill DB, Ferrario CM. Angiotensin II acts at AT1 receptors in the nucleus of the solitary tract to attenuate the baroreceptor reflex. *Am J Physiol.* 1998;275:R1611–R1619.
27. Abdel-Rahman AA, Tao S. Differential alteration of neuronal and cardiovascular responses to adenosine microinjected into the nucleus tractus solitarius of spontaneously hypertensive rats. *Hypertension.* 1996;27:939–948.
28. Tsukamoto K, Sved AF, Ito S, Komatsu K, Kanmatsuse K. Enhanced serotonin-mediated responses in the nucleus tractus solitarius of spontaneously hypertensive rats. *Brain Res.* 2000;863:1–8.
29. Folkow B. Physiological aspects of primary hypertension. *Physiol Rev.* 1982;62:347–504.
30. Kimura K, Ito M, Amano M, Chihara K, Fukata Y, Nakafuku M, Yamamori B, Feng J, Nakano T, Okawa K, Iwamatsu A, Kaibuchi K. Regulation of myosin phosphatase by Rho and Rho-associated kinase (Rho-kinase). *Science.* 1996;273:245–248.
31. Kawano Y, Fukata Y, Oshiro N, Amano M, Nakamura T, Ito M, Matsumura F, Inagaki M, Kaibuchi K. Phosphorylation of myosin binding subunit(MBS) of myosin phosphatase by Rho-kinase in vivo. *J Cell Biol.* 1999;147:1023–1037.
32. Aicher SA, Sharma S, Mitchell JL. Structural changes in AMPA-receptive neurons in the nucleus of the solitary tract of spontaneously hypertensive rats. *Hypertension.* 2003;41:1246–1252.

Circulation
JOURNAL OF THE AMERICAN HEART ASSOCIATION

American Heart Association®
Learn and Live℠

Overexpression of Mitochondrial Transcription Factor A Ameliorates Mitochondrial Deficiencies and Cardiac Failure After Myocardial Infarction

Masaki Ikeuchi, Hidenori Matsusaka, Dongchon Kang, Shouji Matsushima, Tomomi Ide, Toru Kubota, Toshiyuki Fujiwara, Naotaka Hamasaki, Akira Takeshita, Kenji Sunagawa and Hiroyuki Tsutsui

Circulation 2005;112;683-690; originally published online Jul 25, 2005;
DOI: 10.1161/CIRCULATIONAHA.104.524835
Circulation is published by the American Heart Association. 7272 Greenville Avenue, Dallas, TX 72514
 Print ISSN: 0009-7322. Online ISSN: 1524-4539

Overexpression of Mitochondrial Transcription Factor A Ameliorates Mitochondrial Deficiencies and Cardiac Failure After Myocardial Infarction

Masaki Ikeuchi, MD; Hidenori Matsusaka, MD; Dongchon Kang, MD, PhD; Shouji Matsushima, MD; Tomomi Ide, MD, PhD; Toru Kubota, MD, PhD; Toshiyuki Fujiwara, MD, PhD; Naotaka Hamasaki, MD, PhD; Akira Takeshita, MD, PhD; Kenji Sunagawa, MD, PhD; Hiroyuki Tsutsui, MD, PhD

Background—Mitochondrial DNA (mtDNA) copy number is decreased not only in mtDNA-mutation diseases but also in a wide variety of acquired degenerative and ischemic diseases. Mitochondrial transcription factor A (TFAM) is essential for mtDNA transcription and replication. Myocardial mtDNA copy number and TFAM expression both decreased in cardiac failure. However, the functional significance of TFAM has not been established in this disease state.

Methods and Results—We have now addressed this question by creating transgenic (Tg) mice that overexpress human *TFAM* gene and examined whether TFAM could protect the heart from mtDNA deficiencies and attenuate left ventricular (LV) remodeling and failure after myocardial infarction (MI) created by ligating the left coronary artery. *TFAM* overexpression could ameliorate the decrease in mtDNA copy number and mitochondrial complex enzyme activities in post-MI hearts. Survival rate during 4 weeks of MI was significantly higher in Tg-MI than in wild-type (WT) littermates (WT-MI), although infarct size was comparable. LV cavity dilatation and dysfunction were significantly attenuated in Tg-MI. LV end-diastolic pressure was increased in WT-MI, and it was also reduced in Tg-MI. Improvement of LV function in Tg-MI was accompanied by a decrease in myocyte hypertrophy, apoptosis, and interstitial fibrosis as well as oxidative stress in the noninfarcted LV.

Conclusions—Overexpression of *TFAM* inhibited LV remodeling after MI. TFAM may provide a novel therapeutic strategy of cardiac failure. (***Circulation.* 2005;112:683-690.**)

Key Words: free radicals ■ genes ■ heart failure ■ myocardial infarction ■ remodeling

Myocardial infarction (MI) leads to complex structural alterations (remodeling) involving both the infarcted and noninfarcted left ventricular (LV) myocardium. Early remodeling is LV cavity dilatation occurring during the early phase of MI, which is likely due to wall thinning of the infarct region. During the first several days, LV enlargement follows, and thereafter a progressive dilatation of the noninfarcted LV associated with myocyte hypertrophy and interstitial fibrosis occurs over weeks. These progressive changes in LV geometry contribute to the development of depressed cardiac function, clinical heart failure, and increased mortality. Accordingly, it is of critical importance to explore the mechanisms and to develop therapeutic strategies that will effectively inhibit this deleterious process.

Mitochondria have their own genomic system, mitochondrial DNA (mtDNA), a closed-circular double-stranded DNA molecule. MtDNA contains 2 promoters, the light-strand and heavy-strand promoters (LSP and HSP, respectively), from which transcripts are produced and then processed to yield the individual mRNAs encoding 13 subunits of the oxidative phosphorylation system, ribosomal and transfer RNAs.[1,2] Transcription from the LSP also produces RNA primer, which is necessary for initiating mtDNA replication. Mitochondrial function is controlled by the mtDNA as well as factors that regulate mtDNA transcription and/or replication.[3] This raises the possibility that mitochondrial gene replication and thus the mitochondrial DNA copy number and/or mitochondrial gene transcription are impaired in heart failure. Indeed, heart failure is frequently associated with qualitative and quantitative defects in mtDNA.[4–7] Recently, we demonstrated that the decline in mitochondrial function and mtDNA copy number plays a major role in the development of heart failure that occurs after MI.[8,9]

Received November 30, 2004; revision received April 17, 2005; accepted April 22, 2005.

From the Department of Cardiovascular Medicine (M.I., H.M., S.M., T.I., T.K., A.T., K.S.) and Clinical Chemistry and Laboratory Medicine (D.K., N.H.), Graduate School of Medical Sciences, Kyushu University, Fukuoka; Department of Biochemistry, Fukuoka University School of Medicine, Fukuoka (T.F.); and Department of Cardiovascular Medicine, Hokkaido University Graduate School of Medicine, Sapporo (H.T.), Japan.

Online-only Data Supplements I and II can be found at http://circ.ahajournals.org/cgi/content/full/CIRCULATIONAHA.104.524835/DC1.

Correspondence to Hiroyuki Tsutsui, MD, PhD, Department of Cardiovascular Medicine, Hokkaido University Graduate School of Medicine, Kita-15, Nishi-7, Kita-ku, Sapporo 060-8638, Japan. E-mail htsutsui@med.hokudai.ac.jp

Circulation **is available at http://www.circulationaha.org** **DOI: 10.1161/CIRCULATIONAHA.104.524835**

Mitochondrial transcription factor A (TFAM) is a nucleus-encoded protein that binds upstream of the LSP and HSP of mtDNA and promotes transcription of mtDNA. It also plays an important role in regulating mtDNA copy number.[10] In fact, disruption of the *Tfam* gene in mice causes depletion of mtDNA, loss of mitochondrial transcripts, loss of mtDNA-encoded polypeptides, and severe respiratory chain deficiency.[11] Moreover, targeted disruption of *Tfam* in cardiac myocytes induced deletion of mtDNA and dilated cardiomyopathy.[12,13] These lines of evidence obtained from knockout mice have established a critical role for TFAM in regulation of mtDNA copy number and mitochondrial function as well as maintenance of the physiological function of the heart in vivo. In addition, a reduction in TFAM expression has been demonstrated in several forms of cardiac failure.[7,9,14,15] Therefore, an increase in *TFAM* expression may exert beneficial effects on cardiac remodeling after MI. However, it has not yet been analyzed whether an increase in *TFAM* expression can ameliorate mitochondrial dysfunction in heart failure and whether this protein may have therapeutic potential. To address these questions, we created transgenic (Tg) mice containing human *TFAM* gene. Accordingly, human *TFAM* Tg mice and their wild-type (WT) littermates were randomized to have either a large transmural MI induced by coronary artery ligation or sham operation.

Methods

Generation of Tg Mice

Human *TFAM* cDNA was inserted into the unique *Eco*RI site between the CAG (modified chicken β-actin promoter with CMV-IE enhancer) promoter and 3′-flanking sequence of the rabbit β-globin gene of the pCAGGS expression vector[16] and used to generate Tg mice (Figure 1A). The pronuclei of fertilized eggs from hyperovulated C57BL/6 mice were microinjected with this DNA construct. The presence of the *TFAM* transgene was confirmed by polymerase chain reaction (PCR) before the experiments. Four independent founder lines were identified and mated to C57BL/6 WT mice to generate pure C57BL/6 genetic background WT and Tg offspring. Heterozygous Tg mice were used at 10 to 13 weeks of age. The study was approved by our Institutional Animal Research Committee and conformed to the animal care guidelines of the American Physiological Society.

Western Blotting

The protein levels human TFAM and mouse Tfam were analyzed in cardiac tissue homogenates by Western blot analysis with a polyclonal antiserum against human TFAM and mouse Tfam, respectively. In brief, the LV tissues were homogenized with the lysis buffer (1% SDS, 1.0 mmol/L sodium orthovanadate, 10 mmol/L Tris; pH 7.4). After centrifugation, equal amounts of protein (5 μg protein per lane), estimated by the Bradford method with the use of a protein assay (Bio-Rad), were electrophoresed on a 12.5% SDS–polyacrylamide gel and then electrophoretically transferred to a nitrocellulose membrane (Millipore). After blocking with 5% nonfat milk in PBS containing 0.05% Tween-20 at 4°C overnight, the membrane was incubated with the first antibody and then with the peroxidase-linked second antibody (Amersham Pharmacia). Chemiluminescence was detected with an ECL Western blot detection kit (Amersham Pharmacia) according to the manufacturer's recommendation.

Immunohistochemistry

Frozen sections of cardiac tissues were incubated in the presence of 100 nmol/L Mitotracker Red CMXRos (Molecular Probes) at 37°C for 20 minutes. We did not repeat freezing-thawing to avoid the loss of mitochondrial integrity. After they were washed with PBS (10 mmol/L sodium phosphate, pH 7.4, and 150 mmol/L NaCl), the sections were fixed with 3.7% formaldehyde for 5 minutes. After they were washed, the fixed sections were incubated with 100-fold diluted anti-TFAM affinity purified antibodies (10 μg/mL) in PBS at 4°C overnight. Fluorescence images were taken with a confocal laser scanning microscope (Bio-Rad MRC 1000) with laser beams of 488 and 568 nm for excitation.

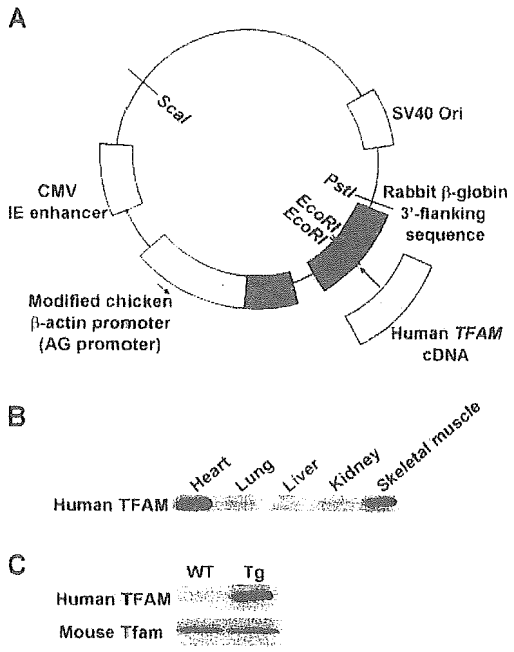

Figure 1. Characterization of human *TFAM* Tg mice. A, Diagram of the human *TFAM* transgenic construct. Plasmid was constructed by inserting a human *TFAM* cDNA (0.74 kb) into the unique *Eco*RI site between the CAG promoter and 3′-flanking sequence of the rabbit β-globin gene of the pCAGGS expression vector. Tg mice harboring human *TFAM* cDNA were identified by PCR with genomic DNA prepared from tail biopsies. CMV indicates cytomegalovirus; IE, immediate early; SV40, simian virus; and Ori, origin of DNA replication. B, Western blot analysis of human TFAM protein in various tissues from Tg mice. Total protein extracts from heart, lung, liver, kidney, and skeletal muscle were probed with a polyclonal antiserum against human TFAM. The antibody recognized TFAM as a single band of 24 kDa. C, Western blot analysis of human TFAM and mouse Tfam protein levels in the heart from Tg and WT mice.

Creation of MI

We created MI in mice by ligating the left coronary artery. Sham operation without coronary artery ligation was also performed.[9] Tail clips were applied, and a PCR protocol was performed to confirm the genotype by a group of investigators. Next, MI was induced in these mice by another subset of investigators, who were not informed of the genotyping results. This assignment procedure was performed with numeric codes to identify the animals.

Survival

To perform the survival analysis, cages were inspected for deceased animals during the study period of 4 weeks. All deceased mice were examined for the presence of MI as well as pleural effusion and cardiac rupture.

We performed the subsequent molecular (mtDNA copy number and mtRNA), biochemical (mitochondrial enzyme activity and apoptosis), and histopathological (myocyte cross-sectional area, collagen volume fraction, and mitochondrial ultrastructure) analysis by using the LV from sham-operated mice and the noninfarcted LV from MI mice.

Southern Blot Analysis

DNA was extracted from cardiac tissues, and a Southern blot analysis was performed to measure the mtDNA copy number as described earlier.[9] Primers for the mtDNA probe corresponded to nucleotides 2424 to 3605 of the mouse mitochondrial genome, and those for the nuclear-encoded mouse 18S rRNA probe corresponded to nucleotides 435 to 1951 of the human 18S rRNA genome. The mtDNA levels were normalized to the abundance of the 18S rRNA gene run on the same gel.

RNA Isolation and Northern Blot Analysis

Total RNA was isolated from frozen LV by the guanidinium method, and a Northern hybridization analysis was performed according to methods described previously.[9] Probes for mtRNA analysis were prepared by amplification of nucleotides 1209 to 2606 (probe 1), nucleotides 3351 to 7570 (probe 2), nucleotides 8861 to 14549 (probe 3), and nucleotides 14729 to 15837 (probe 4) of mtDNA from mouse genomic DNA.

Mitochondrial Enzyme Activity

The specific activity of complex I, complex II, complex III, and complex IV was measured in the myocardial tissues according to methods described previously.[9] The specific enzymatic activity of rotenone-sensitive NADH-ubiquinone oxidoreductase (complex I) was measured by a reduction of the ubiquinone analogue decylubiquinone. For the activity of succinate-ubiquinone oxidoreductase (complex II), the reduction of 2,6-dichlorophenolindophenol, when coupled to complex II–catalyzed reduction of decylubiquinone, was measured. For the specific activity of ubiquinol/cytochrome *c* oxidoreductase (complex III), the reduction of cytochrome *c* catalyzed by complex III in the presence of reduced decylubiquinone was monitored. The specific activity of cytochrome *c* oxidase (complex IV) was measured by following the oxidation of reduced cytochrome *c*, which had been prepared in the presence of dithionite. All enzymatic activities were expressed as nanomoles per minute per milligram protein.

Echocardiographic and Hemodynamic Measurements

After 4 weeks of surgery, echocardiographic studies were performed under light anesthesia with tribromoethanol/amylene hydrate (Avertin; 2.5% wt/vol, 8 μL/g IP) and spontaneous respiration. A 2D parasternal short-axis view of the LV was obtained at the level of the papillary muscles. In general, the best views were obtained with the transducer lightly applied to the mid upper left anterior chest wall. The transducer was then gently moved cephalad or caudad and angulated until desirable images were obtained. After it was ensured that the imaging was on axis (based on roundness of the LV cavity), 2D targeted M-mode tracings were recorded at a paper speed of 50 mm/s. Our previous study has shown that the intraobserver and interobserver variabilities of our echocardiographic measurements for LV dimensions were small, and measurements made in the same animals on separate days were highly reproducible.[17] Then, under the same anesthesia with Avertin, a 1.4F micromanometer-tipped catheter (Millar Instruments) was inserted into the right carotid artery and then advanced into the LV to measure pressures.[17]

Infarct Size

To measure the infarct size after 28 days of MI, the heart was excised, and the LVs were cut from apex to base into 3 transverse sections. Five-micrometer sections were cut and stained with Masson's trichrome. Infarct length was measured along the endocardial and epicardial surfaces from each of the cardiac sections, and the values from all specimens were summed. Infarct size (in percentage) was calculated as total infarct circumference divided by total cardiac circumference.[17]

In addition, to measure infarct size after 24 hours when most animals are still alive, a separate group of animals including WT-MI (n=6) and Tg-MI (n=6) was created. After 24 hours of coronary artery ligation, Evans blue dye (1%) was perfused into the aorta and coronary arteries, and tissue sections were weighed and then incubated with a 1.5% triphenyltetrazolium chloride solution. The infarct area (pale), the area at risk (not blue), and the total LV area from each section were measured.[18] In our preliminary study, we confirmed excellent reliability of infarct size measurements, in which a morphometric methodology similar to that used in this study was used. The intraobserver and interobserver variabilities between 2 measurements divided by these means, expressed as a percentage, were <5%.

Histopathology

After in vivo hemodynamic studies, the heart was excised and dissected into the right and left ventricles, including the septum. Five-micrometer sections were cut and stained with Masson's trichrome. Myocyte cross-sectional area and collagen volume fraction were determined by the quantitative morphometry of LV tissue sections.[17]

For assessment of mitochondrial ultrastructure by electron microscopy, LV tissues were fixed in a mixture of 1% glutaraldehyde and 4% paraformaldehyde in 0.1 mol/L phosphate buffer at pH 7.4 for 2 hours at room temperature. After they were washed in 0.1 mol/L phosphate buffer containing 0.25 mol/L sucrose, they were postfixed with 1% osmium tetroxide for 1 hour at room temperature. The tissues were then block-stained with 1% uranyl acetate in 50% methanol for 2 hours, dehydrated in a graded series of ethanol, and embedded in Epon. Ultrathin sections were double stained with uranyl acetate and lead citrate and then were observed under an electron microscope (Hitachi H7000). For quantitative morphometric analysis, the number and size of the mitochondria were examined according to methods described previously.[9] The number of mitochondria and the cross-sectional area (size) of each mitochondrion were measured within a sampling region of 100 square sarcomeres (sm^2). Eighteen regions were selected at random for each specimen, and for all regions the averages of mitochondrial number and cross-sectional area were calculated.

Apoptosis

To detect apoptosis, LV tissue sections were stained with terminal deoxynucleotidyl transferase–mediated dUTP nick end-labeling (TUNEL) staining. The number of TUNEL-positive cardiac myocyte nuclei was counted, and the data were normalized per 10^5 total nuclei identified by hematoxylin-positive staining in the same sections. We further examined whether apoptosis is present by the more sensitive ligation-mediated PCR fragmentation assays (Maxim Biotech Inc).[18]

Statistical Analysis

Data are expressed as mean±SEM. Survival analysis was performed by the Kaplan-Meier method, and between-group difference in survival was tested by the log-rank test. Between-group comparison of means was performed by 1-way ANOVA, followed by *t* tests. The Bonferroni correction was done for multiple comparisons of means. $P<0.05$ was considered statistically significant.

Results

Characterization of Human TFAM Tg Mice

Human *TFAM* cDNA was used to generate Tg mice (Figure 1A). Four lines of Tg mice were confirmed by PCR. These lines were viable and fertile, and there were no detectable differences in cardiac size and structure between Tg and WT mice either macroscopically or microscopically.

We analyzed TFAM protein levels in various tissues by Western blot analysis using anti-human TFAM antibody. We found a robust expression of human TFAM protein in the heart and skeletal muscle, but it was barely detected in the lung, liver, and kidney (Figure 1B). Among 4 established lines of Tg mice, 1 line that expressed the highest level of the human TFAM protein in the heart was used for further

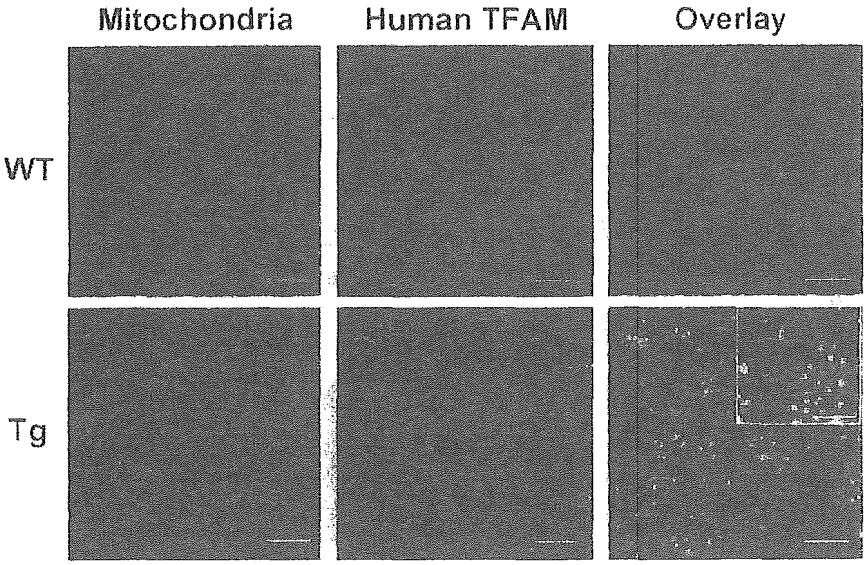

Figure 2. Myocardial tissue sections from WT (top) and Tg (bottom) mice were double-stained with MitoTracker dye (red) and a human TFAM specific antibody (green). Immunoreactivity for human TFAM was observed in the cytoplasm of cardiac myocytes. Merged images show that TFAM was colocalized with the mitochondria (yellow). Bar=20 μm. Inset shows merged images with higher magnification; bar=10 μm.

experiments. The endogenous expression level of the mouse Tfam protein was not modified or downregulated by the overexpression of human *TFAM* gene (Figure 1C). Immunohistochemical studies showed homogeneous human TFAM distribution in cardiac myocytes and colocalized with the mouse mitochondria (Figure 2). Human TFAM staining showed a relatively spotty staining pattern. With higher magnification, its expression appeared not to be restricted to a specific site of mitochondria (Figure 2, inset). These results suggest that the human TFAM exerts an expression pattern similar to that observed for the endogenous mouse Tfam and may function in the mouse heart.

MtDNA Copy Number and Mitochondrial Enzymes

We created MI in male Tg mice (Tg-MI) and nontransgenic wild-type littermates (WT-MI). Sham operation without coronary artery ligation was also performed in WT (WT-sham) and Tg (Tg-sham) mice. After 4 weeks of surgery, we measured mtDNA copy number, expressed as the ratio of mtDNA to nuclear DNA (18S rRNA), in the myocardial tissue by a Southern blot analysis. In parallel to an increase in TFAM protein, mtDNA copy number increased in the heart from Tg animals compared with WT controls (Figure 3A). In WT-MI animals, mtDNA copy number in the noninfarcted LV showed a 41% decrease ($P<0.01$) compared with sham mice, which was significantly prevented and preserved at a normal level in Tg-MI mice (Figure 3A).

To determine the effects of mtDNA copy number alterations on mtRNA, mtRNA transcript levels were measured by Northern blot analysis. As previously reported,[9] mtRNA transcript levels, including ND1+ND2, ND4, ND4L, ND5, cytochrome *b*, COI, COII, and COIII transcripts as well as 16S rRNA, were lower in WT-MI than those in WT-sham. However, overexpression of human *TFAM* did not increase, and even decreased, these mRNA levels in Tg-sham as well as in Tg-MI (online-only Data Supplement I). These results indicate that the regulation of mtRNA transcripts is dissociated from that of mtDNA copy number.

We next measured the respiratory chain enzyme activities. Despite the significant increase in mtDNA copy number in the heart from Tg, complex I, complex II, complex III, and complex IV demonstrated no significant changes in the enzymatic activity in comparison with WT controls (Figure 3B). Consistent with mtDNA copy number, the enzymatic activities of complex I, complex III, and complex IV were significantly lower in the noninfarcted LV from WT-MI than those from WT-sham. Most importantly, there was no such decrease observed in Tg-MI (Figure 3B). The enzymatic activity of complex II, exclusively encoded by nuclear DNA, was not altered in either group. These results indicate that mtDNA and mitochondrial enzymatic activities are downregulated in the hearts after MI, and human *TFAM* gene overexpression efficiently counteracts these mitochondrial deficiencies.

The overall number of mitochondria and the overall average size of the mitochondria demonstrated no significant changes in Tg-sham in comparison with WT controls. In contrast, the mitochondrial number was significantly increased and their size was decreased in WT-MI, both of which were attenuated in Tg-MI (online-only Data Supplement II).

Survival

The survival analysis was performed in 4 groups of mice during the study period of 4 weeks; WT-sham (n=20), WT-MI (n=21), Tg-sham (n=29), and Tg-MI (n=29). There were no deaths in sham-operated groups. The survival rate was significantly higher in Tg-MI compared with WT-MI (100% versus 66%; $P<0.01$; Figure 4A).

Infarct Size

We determined the infarct size by morphometric analysis in the surviving mice 28 days after MI, and it was comparable between WT-MI and Tg-MI (Figure 4B). To further confirm that overexpression of *TFAM* gene did not alter the infarct size, both area at risk and infarct area were measured in a separate group of mice 24 hours after coronary artery ligation.

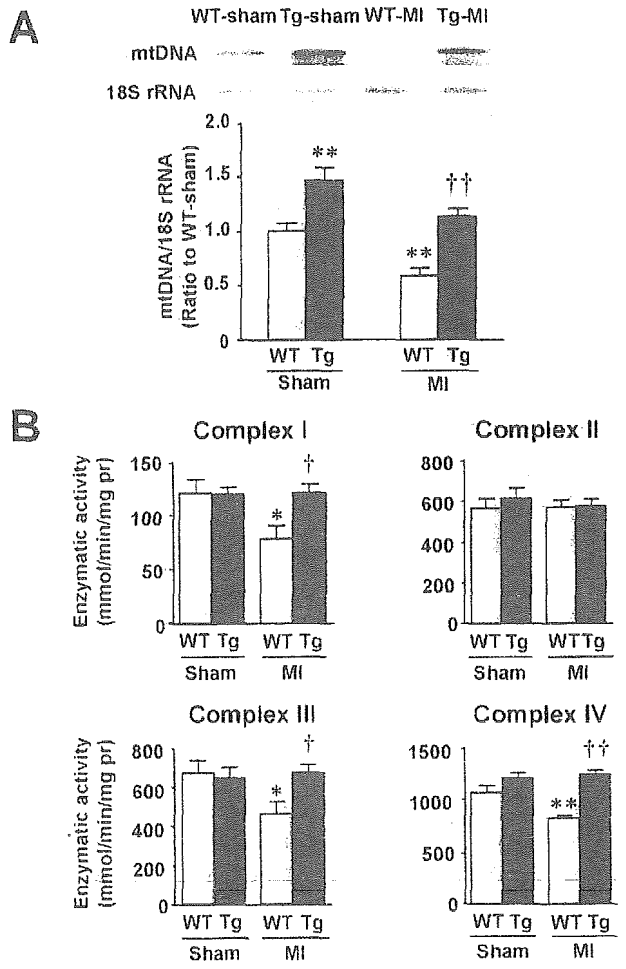

Figure 3. mtDNA and mitochondrial function. A, top, Southern blot analysis of mtDNA copy number in total DNA extracts from the heart from WT-sham, Tg-sham, WT-MI, and Tg-MI mice. Top bands show signals from the mtDNA fragment, and bottom bands show signals from the nuclear DNA fragment containing the 18S rRNA gene. A, bottom, Summary data for a Southern blot analysis of mtDNA copy number in 4 groups of animals (n=8 for each). Data were obtained by a densitometric quantification of the Southern blots such as those shown in A. B, Enzymatic activity of respiratory chain complex I, complex II, complex III, and complex IV in isolated mitochondria from 4 groups of animals (n=6 for each). Each assay was done in triplicate. Values are mean±SEM. *$P<0.05$, **$P<0.01$ for difference from WT-sham values. †$P<0.05$, ††$P<0.01$ for difference from WT-MI values. pr indicates protein.

The infarct size (infarct/risk area) was also comparable between WT-MI and Tg-MI mice (84.5±0.4% for n=6 versus 83.2±1.1% for n=6; P=NS; Figure 4C).

Cardiac Function and Structure

The echocardiographic studies of surviving mice at 4 weeks showed that cardiac diameters were significantly increased in WT-MI over the values in WT-sham or Tg-sham. Tg-MI showed less cavity dilatation and improved contractile function compared with WT-MI (Figure 5).

There was no significant difference in heart rate and aortic blood pressure among 4 groups of mice (Table). LV end-diastolic pressure increased in WT-MI and was significantly attenuated in Tg-MI. Coinciding with increased LV end-diastolic pressure, lung weight/body weight increased in WT-MI

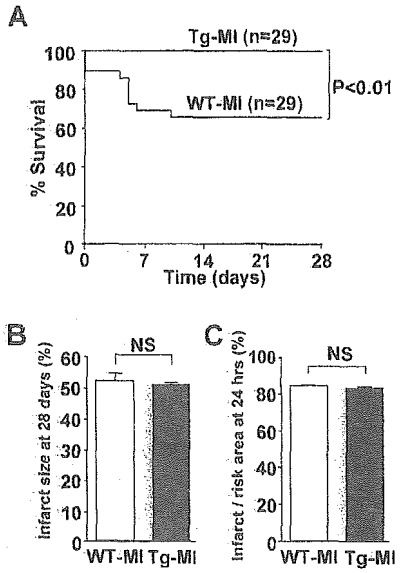

Figure 4. Survival and infarct size. A, Kaplan-Meier survival analysis. Percentages of surviving WT-MI (n=29) and Tg-MI (n=29) mice were plotted. Between-group difference was tested by the log-rank test. B, Infarct size values from WT-MI (n=6) and Tg-MI (n=6) mice in surviving mice 28 days after MI. C, Infarct size (infarct/risk area) values from WT-MI (n=6) and Tg-MI (n=6) mice 24 hours after MI. Values are mean±SEM.

and was also attenuated in Tg-MI (Table). The prevalence of pleural effusion, a clinical sign of heart failure, was significantly lower in Tg-MI than that in WT-MI (Table).

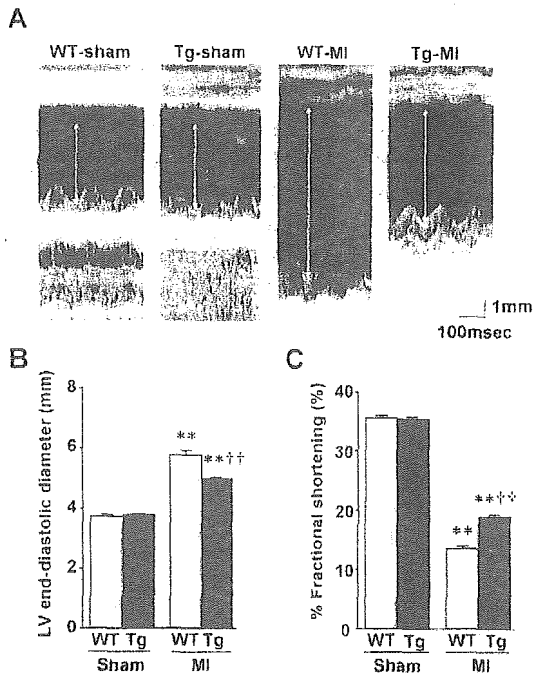

Figure 5. A, Representative M-mode echocardiograms obtained from WT-sham, Tg-sham, WT-MI, and Tg-MI mice. Arrows indicate LV end-diastolic diameter. B, C, Summary data for echocardiographic measurements in 4 groups of animals (n=6 for each). LV end-diastolic diameter (B) and percent fractional shortening (C) are shown. Values are mean±SEM. **$P<0.01$ for difference from WT-sham values; ††$P<0.01$ for difference from WT-MI values.

Characteristics of Animal Models

	WT-Sham (n=20)	Tg-Sham (n=21)	WT-MI (n=19)	Tg-MI (n=29)
Hemodynamic data				
Heart rate, bpm	469±6	471±4	479±11	477±4
Mean aortic pressure, mm Hg	77±4	76±2	73±1	74±1
LV EDP, mm Hg	0.7±0.5	0.7±0.4	13.1±2.0**	4.3±0.8*‡
Organ weight data				
Body weight, g	27.3±0.4	26.7±0.4	26.2±0.5	26.0±0.2
LV weight/body weight, mg/g	3.14±0.07	3.23±0.05	3.88±0.24**	3.69±0.09**
RV weight/body weight, mg/g	0.95±0.05	0.98±0.04	1.39±0.12**	1.12±0.05†
Lung weight/body weight, mg/g	5.3±0.1	5.3±0.1	8.3±0.6**	6.4±0.3‡
Pleural effusion, %	0	0	63**	31**†

Values are mean±SEM. EDP indicates end-diastolic pressure; RV, right ventricular.
**$P<0.01$ vs WT-sham; †$P<0.05$, ‡$P<0.01$ vs WT-MI.

Cross-sectional area of cardiac myocytes, an index of cellular hypertrophy, increased in the noninfarcted LV from WT-MI and was significantly attenuated in Tg-MI (Figure 6A). Collagen volume fraction, an index of myocardial interstitial fibrosis, also increased in the noninfarcted LV from WT-MI and was significantly smaller in Tg-MI (Figure 6B). These results indicate that TFAM efficiently counteracts structural and functional deterioration in post-MI hearts.

Apoptosis

To detect apoptosis, myocardial tissue sections were stained with TUNEL staining. TUNEL-positive nuclei were rarely seen in control mice, whereas their number increased in the noninfarcted LV from WT-MI and was significantly decreased in Tg-MI (Figure 7A). In addition, DNA ladder appeared faint in the noninfarcted LV from Tg-MI compared with that from WT-MI, suggesting the attenuation of apoptosis by *TFAM* overexpression (Figure 7B).

Discussion

The present study provides the first direct evidence that the overexpression of *TFAM* can prevent the decline in mtDNA as well as mitochondrial respiratory defects in post-MI hearts. TFAM significantly attenuated cardiac chamber dilatation and dysfunction as well as histopathological changes such as myocyte hypertrophy, interstitial fibrosis, and apoptosis. The apparent beneficial effects of *TFAM* overexpression were not due to its MI size–sparing effect, but they occurred secondary to more adaptive remodeling. All of these beneficial effects could contribute to the improved survival in Tg mice after MI.

Previous studies have suggested an intimate link between mtDNA damage, increased lipid peroxidation, and a decrease in mitochondrial electron transport complex enzyme activities.[4] A growing body of evidence suggests that mtDNA deficiencies and mitochondrial dysfunction play a major role in the development and progression of cardiac failure. A recent study from our laboratory demonstrated a decline in TFAM and mtDNA copy number in a murine heart failure model after MI.[9] These studies imply a relationship between TFAM, mtDNA copy

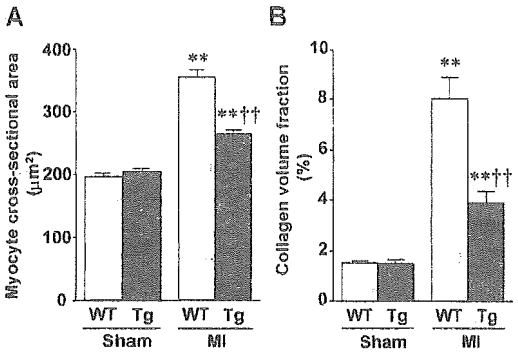

Figure 6. Summary data for histopathological analysis of LV tissue sections in 4 groups of animals (n=6 for each). Myocyte cross-sectional area (A) and collagen volume fraction (B) are shown. Values are mean±SEM. **$P<0.01$ for difference from WT-sham values; ††$P<0.01$ for difference from WT-MI values.

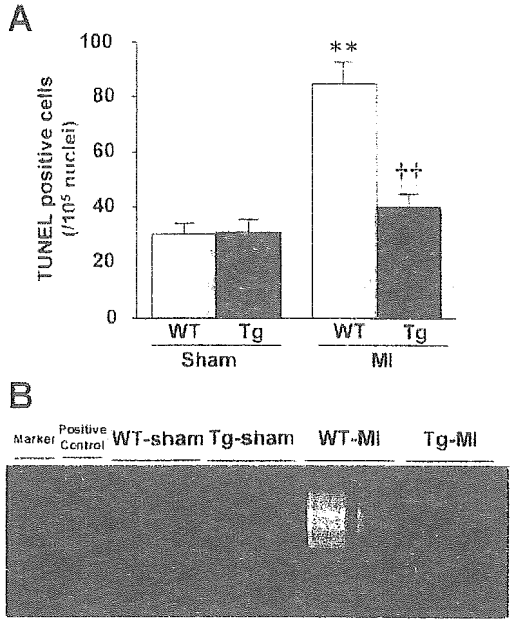

Figure 7. A, Number of TUNEL-positive myocytes in noninfarcted area of LV from 4 groups of animals (n=8 each). Values are mean±SEM. **$P<0.01$ for difference from WT-sham values. ††$P<0.01$ for difference from WT-MI values. B, DNA ladder indicative of apoptosis in genomic DNA from LV.

number, and mitochondrial function because the magnitude of the mtDNA defects is parallel to quantitative deficiencies in electron transport function. We thus proposed a direct relationship between TFAM content and electron transport chain activity during the post-MI remodeling process, ignoring the possibility of direct ischemic damage to the electron transport chain complexes. The downregulation of *TFAM* gene expression and a concurrent decrease in mitochondrial genes have been also shown in heart failure induced by aortic banding.[15] In addition, mtDNA depletion has been reported in mitochondrial myopathy and respiratory defects.[19–21] On the basis of these studies, mtDNA defects are considered to be involved not only in the pathogenesis of the diseases caused by inherited defects of mtDNA but also in those secondary to ischemia or mechanical overload.

TFAM not only regulates mtDNA transcription and replication[22] but also maintains mtDNA copy number. In fact, *Tfam* knockout mice, which had a 50% reduction in their transcript and protein levels, exerted a 34% reduction in the mtDNA copy number, 22% reduction in the mitochondrial transcript levels, and partial reduction in the cytochrome *c* oxidase levels in the heart.[11] Moreover, cardiac-specific disruption in the *Tfam* gene in mice exhibited dilated cardiomyopathy in association with a reduced amount of mtDNA and mitochondrial transcripts.[13] The transfection of antisense plasmids in culture, designed to reduce the expression of *TFAM*, effectively decreased the levels of mitochondrially encoded transcripts.[23] On the contrary, the forced overexpression of *TFAM* could produce the opposite effect.[24] Consistent with the present results (Figure 3A, 3B), a recent study by Ekstrand et al[25] demonstrated that the overexpression of human *TFAM* in the mouse increased mtDNA copy number. These lines of evidence imply the primary importance of TFAM as a regulatory mechanism of mtDNA copy number. TFAM has been shown to directly interact with mtDNA to form nucleoids.[26,27] Therefore, increased TFAM may increase the steady-state levels of mtDNA by directly binding and stabilizing mtDNA in Tg-sham mice. Our study also showed that overexpression of human *TFAM* did not increase the respiratory chain complex enzyme activities in Tg-sham mice (Figure 3C), suggesting that the regulation of mtDNA copy number is dissociated from that of electron transport function.[25] Furthermore, our proposed association between TFAM, mtDNA copy number, and electron transport chain activity may be weakened by our data that *TFAM* overexpression did not affect mtRNA levels (online-only Data Supplement I). There may be complex regulatory mechanisms responsible for the association of TFAM, mtDNA, and mitochondrial function, and further studies are clearly needed to solve this issue.

The results obtained from human *TFAM* Tg-sham mice differ from those from the inducible, cardiac-specific overexpression of peroxisome proliferator-activated receptor γ coactivator-1α (PGC-1α) transgene in adult mice, which leads to a modest increase in mitochondrial number and development of reversible cardiomyopathy.[28] PGC-1α is the transcriptional coactivator and acts upstream of TFAM and also has the capacity to increase mtDNA levels as well as mitochondrial mass in cultured cells and in Tg mice.[29,30] The reason for the discrepant results between PGC-1 and TFAM transgene overexpression remains unsolved in this study, which, however, may be related to the complex regulatory mechanisms of mitochondrial biogenesis and function by PGC-1 and its downstream factors, including nuclear respiratory factors 1 and 2 and TFAM.[31,32] This may also be due to the difference in the timing of transgene overexpression. Moreover, even though the present study demonstrated the beneficial effects of *TFAM* overexpression on post-MI LV remodeling, it could not determine whether it must occur before the ischemic insult or only during the post-MI phase.

The present study clearly demonstrated that *TFAM* overexpression could ameliorate the decline in mtDNA copy number and preserve it at a normal level in hearts from Tg-MI mice (Figure 3A). *TFAM* overexpression might increase the steady-state levels of mtDNA by directly stabilizing mtDNA. Consistent with alterations in mtDNA, the decrease in oxidative capacities seen in MI was also prevented (Figure 3B). Moreover, our studies establish an important role of TFAM in myocardial protection against remodeling and failure (Figures 4A and 5). The beneficial effects of *TFAM* overexpression shown in the present study were not due to its MI size–sparing effect because infarct size was comparable between WT-MI and Tg-MI mice (Figure 4B, 4C). Furthermore, its effects were not due to the effects on hemodynamics because blood pressure and heart rate were not altered (Table).

Several factors may be attributable to the protective effects conferred by TFAM against myocardial remodeling and failure. First, *TFAM* overexpression prevented the decrease in mtDNA copy number (Figure 3A) and mitochondrial electron transport function (Figure 3B), which may contribute to the decrease in myocardial oxidative stress. The decreased oxidative stress could contribute to the amelioration of cardiac hypertrophy, apoptosis, and interstitial fibrosis.[18] Second, *TFAM* overexpression may induce mitochondrial biogenesis, which, however, is thought to be unlikely because the number and size of the mitochondria assessed by electron microscopy were not altered in Tg-sham mice (online-only Data Supplement II). Importantly, the beneficial effects of *TFAM* overexpression on LV remodeling and failure occurred with the attenuation of increased mitochondrial number seen in MI. Furthermore, an increase in mitochondrial number itself did not necessarily exert beneficial effects in MI.

Several pathogenic mtDNA base substitution mutations, such as missense mutations and mtDNA rearrangement mutations (deletions and insertions), have been identified in patients with mitochondrial diseases.[4] An accumulation of the deleted forms of mtDNA in the myocardium frequently results in either cardiac hypertrophy, conduction block, or heart failure.[33] Furthermore, there is now a consensus view that mutations in mtDNA and abnormalities in mitochondrial function are associated with common forms of cardiac diseases, such as ischemic heart disease[34] and dilated cardiomyopathy.[35] In these conditions, however, the strict causal relationship between abnormalities in mtDNA and cardiac dysfunction has yet to be fully elucidated.

The present study supports our earlier conclusions that the deficiencies of mtDNA contribute to cardiac failure.[9] Furthermore, it confirms that the defects in TFAM are critically involved in mitochondrial dysfunction as well as maladaptive cardiac remodeling and failure. More importantly, the increased

TFAM expression could ameliorate the pathophysiological processes seen in heart failure. MtDNA decline and mitochondrial defects are now well recognized in a variety of diseases such as neurodegenerative diseases, diabetes mellitus, cancer, and even aging. Therefore, with further knowledge on the mechanisms of TFAM for maintenance of mtDNA copy number and mitochondrial function, it may eventually be possible to develop novel strategies for the treatment of such diseases based on the manipulation of TFAM.

Acknowledgments

This study was supported in part by grants from the Ministry of Education, Science, and Culture (Nos. 09670724, 12670676, 14370230). A part of this study was conducted in Kyushu University Station for Collaborative Research I and II.

References

1. Attardi G, Schatz G. Biogenesis of mitochondria. *Annu Rev Cell Biol.* 1988;4:289–333.
2. Shadel GS, Clayton DA. Mitochondrial DNA maintenance in vertebrates. *Annu Rev Biochem.* 1997;66:409–435.
3. Clayton DA. Replication and transcription of vertebrate mitochondrial DNA. *Annu Rev Cell Biol.* 1991;7:453–478.
4. Wallace DC. Mitochondrial diseases in man and mouse. *Science.* 1999; 283:1482–1488.
5. Kajander OA, Karhunen PJ, Jacobs HT. The relationship between somatic mtDNA rearrangements, human heart disease and aging. *Hum Mol Genet.* 2002;11:317–324.
6. Naya FJ, Black BL, Wu H, Bassel-Duby R, Richardson JA, Hill JA, Olson EN. Mitochondrial deficiency and cardiac sudden death in mice lacking the MEF2A transcription factor. *Nat Med.* 2002;8:1303–1309.
7. Lebrecht D, Setzer B, Ketelsen UP, Haberstroh J, Walker UA. Time-dependent and tissue-specific accumulation of mtDNA and respiratory chain defects in chronic doxorubicin cardiomyopathy. *Circulation.* 2003; 108:2423–2429.
8. Ide T, Tsutsui H, Kinugawa S, Utsumi H, Kang D, Hattori N, Uchida K, Arimura K, Egashira K, Takeshita A. Mitochondrial electron transport complex I is a potential source of oxygen free radicals in the failing myocardium. *Circ Res.* 1999;85:357–363.
9. Ide T, Tsutsui H, Hayashidani S, Kang D, Suematsu N, Nakamura K, Utsumi H, Hamasaki N, Takeshita A. Mitochondrial DNA damage and dysfunction associated with oxidative stress in failing hearts after myocardial infarction. *Circ Res.* 2001;88:529–535.
10. Parisi MA, Clayton DA. Similarity of human mitochondrial transcription factor 1 to high mobility group proteins. *Science.* 1991;252:965–969.
11. Larsson NG, Wang J, Wilhelmsson H, Oldfors A, Rustin P, Lewandoski M, Barsh GS, Clayton DA. Mitochondrial transcription factor A is necessary for mtDNA maintenance and embryogenesis in mice. *Nat Genet.* 1998;18:231–236.
12. Li H, Wang J, Wilhelmsson H, Hansson A, Thoren P, Duffy J, Rustin P, Larsson NG. Genetic modification of survival in tissue-specific knockout mice with mitochondrial cardiomyopathy. *Proc Natl Acad Sci U S A.* 2000;97:3467–3472.
13. Wang J, Wilhelmsson H, Graff C, Li H, Oldfors A, Rustin P, Bruning JC, Kahn CR, Clayton DA, Barsh GS, Thoren P, Larsson NG. Dilated cardiomyopathy and atrioventricular conduction blocks induced by heart-specific inactivation of mitochondrial DNA gene expression. *Nat Genet.* 1999;21:133–137.
14. Kanazawa A, Nishio Y, Kashiwagi A, Inagaki H, Kikkawa R, Horiike K. Reduced activity of mtTFA decreases the transcription in mitochondria isolated from diabetic rat heart. *Am J Physiol.* 2002;282:E778–E785.
15. Garnier A, Fortin D, Delomenie C, Momken I, Veksler V, Ventura-Clapier R. Depressed mitochondrial transcription factors and oxidative capacity in rat failing cardiac and skeletal muscles. *J Physiol.* 2003;551: 491–501.
16. Niwa H, Yamamura K, Miyazaki J. Efficient selection for high-expression transfectants with a novel eukaryotic vector. *Gene.* 1991;108: 193–199.
17. Shiomi T, Tsutsui H, Hayashidani S, Suematsu N, Ikeuchi M, Wen J, Ishibashi M, Kubota T, Egashira K, Takeshita A. Pioglitazone, a peroxisome proliferator–activated receptor-gamma agonist, attenuates left ventricular remodeling and failure after experimental myocardial infarction. *Circulation.* 2002;106:3126–3132.
18. Shiomi T, Tsutsui H, Matsusaka H, Murakami K, Hayashidani S, Ikeuchi M, Wen J, Kubota T, Utsumi H, Takeshita A. Overexpression of glutathione peroxidase prevents left ventricular remodeling and failure after myocardial infarction in mice. *Circulation.* 2004;109:544–549.
19. Moraes CT, Shanske S, Tritschler HJ, Aprille JR, Andreetta F, Bonilla E, Schon EA, DiMauro S. mtDNA depletion with variable tissue expression: a novel genetic abnormality in mitochondrial diseases. *Am J Hum Genet.* 1991;48:492–501.
20. Lewis W, Gonzalez B, Chomyn A, Papoian T. Zidovudine induces molecular, biochemical, and ultrastructural changes in rat skeletal muscle mitochondria. *J Clin Invest.* 1992;89:1354–1360.
21. Marin-Garcia J, Goldenthal MJ. Mitochondrial cardiomyopathy: molecular and biochemical analysis. *Pediatr Cardiol.* 1997;18:251–260.
22. Scarpulla RC. Nuclear activators and coactivators in mammalian mitochondrial biogenesis. *Biochim Biophys Acta.* 2002;1576:1–14.
23. Inagaki H, Kitano S, Lin KH, Maeda S, Saito T. Inhibition of mitochondrial gene expression by antisense RNA of mitochondrial transcription factor A (mtTFA). *Biochem Mol Biol Int.* 1998;45:567–573.
24. Montoya J, Perez-Martos A, Garstka HL, Wiesner RJ. Regulation of mitochondrial transcription by mitochondrial transcription factor A. *Mol Cell Biochem.* 1997;174:227–230.
25. Ekstrand MI, Falkenberg M, Rantanen A, Park CB, Gaspari M, Hultenby K, Rustin P, Gustafsson CM, Larsson NG. Mitochondrial transcription factor A regulates mtDNA copy number in mammals. *Hum Mol Genet.* 2004;13:935–944.
26. Alam TI, Kanki T, Muta T, Ukaji K, Abe Y, Nakayama H, Takio K, Hamasaki N, Kang D. Human mitochondrial DNA is packaged with TFAM. *Nucleic Acids Res.* 2003;31:1640–1645.
27. Takamatsu C, Umeda S, Ohsato T, Ohno T, Abe Y, Fukuoh A, Shinagawa H, Hamasaki N, Kang D. Regulation of mitochondrial D-loops by transcription factor A and single-stranded DNA-binding protein. *EMBO Rep.* 2002;3:451–456.
28. Russell LK, Mansfield CM, Lehman JJ, Kovacs A, Courtois M, Saffitz JE, Medeiros DM, Valencik ML, McDonald JA, Kelly DP. Cardiac-specific induction of the transcriptional coactivator peroxisome proliferator-activated receptor gamma coactivator-1alpha promotes mitochondrial biogenesis and reversible cardiomyopathy in a developmental stage-dependent manner. *Circ Res.* 2004;94:525–533.
29. Lin J, Wu H, Tarr PT, Zhang CY, Wu Z, Boss O, Michael LF, Puigserver P, Isotani E, Olson EN, Lowell BB, Bassel-Duby R, Spiegelman BM. Transcriptional co-activator PGC-1 alpha drives the formation of slow-twitch muscle fibres. *Nature.* 2002;418:797–801.
30. Wu Z, Puigserver P, Andersson U, Zhang C, Adelmant G, Mootha V, Troy A, Cinti S, Lowell B, Scarpulla RC, Spiegelman BM. Mechanisms controlling mitochondrial biogenesis and respiration through the thermogenic coactivator PGC-1. *Cell.* 1999;98:115–124.
31. Huss JM, Kelly DP. Nuclear receptor signaling and cardiac energetics. *Circ Res.* 2004;95:568–578.
32. Ventura-Clapier R, Garnier A, Veksler V. Energy metabolism in heart failure. *J Physiol.* 2004;555:1–13.
33. Anan R, Nakagawa M, Miyata M, Higuchi I, Nakao S, Suehara M, Osame M, Tanaka H. Cardiac involvement in mitochondrial diseases: a study on 17 patients with documented mitochondrial DNA defects. *Circulation.* 1995;91:955–961.
34. Corral-Debrinski M, Shoffner JM, Lott MT, Wallace DC. Association of mitochondrial DNA damage with aging and coronary atherosclerotic heart disease. *Mutat Res.* 1992;275:169–180.
35. Arbustini E, Diegoli M, Fasani R, Grasso M, Morbini P, Banchieri N, Bellini O, Dal Bello B, Pilotto A, Magrini G, Campana C, Fortina P, Gavazzi A, Narula J, Vigano M. Mitochondrial DNA mutations and mitochondrial abnormalities in dilated cardiomyopathy. *Am J Pathol.* 1998;153:1501–1510.

Overexpression of eNOS in brain stem reduces enhanced sympathetic drive in mice with myocardial infarction

Koji Sakai, Yoshitaka Hirooka, Hideaki Shigematsu, Takuya Kishi, Koji Ito, Hiroaki Shimokawa, Akira Takeshita and Kenji Sunagawa

AJP - Heart 289:2159-2166, 2005. First published Jul 8, 2005; doi:10.1152/ajpheart.00408.2005

Am J Physiol Heart Circ Physiol 289: H2159–H2166, 2005.
First published July 8, 2005; doi:10.1152/ajpheart.00408.2005.

Overexpression of eNOS in brain stem reduces enhanced sympathetic drive in mice with myocardial infarction

Koji Sakai, Yoshitaka Hirooka, Hideaki Shigematsu, Takuya Kishi, Koji Ito, Hiroaki Shimokawa, Akira Takeshita, and Kenji Sunagawa

Department of Cardiovascular Medicine, Kyushu University Graduate School of Medical Sciences, Fukuoka, Japan

Submitted 25 April 2005; accepted in final form 5 July 2005

Sakai, Koji, Yoshitaka Hirooka, Hideaki Shigematsu, Takuya Kishi, Koji Ito, Hiroaki Shimokawa, Akira Takeshita, and Kenji Sunagawa. Overexpression of eNOS in brain stem reduces enhanced sympathetic drive in mice with myocardial infarction. *Am J Physiol Heart Circ Physiol* 289: H2159–H2166, 2005. First published July 8, 2005; doi:10.1152/ajpheart.00408.2005.—Reduced nitric oxide (NO) in the brain might contribute to enhanced sympathetic drive in heart failure (HF). The aim of this study was to determine whether increased NO production induced by local overexpression of endothelial NO synthase (eNOS) in the nucleus tractus solitarius (NTS) of the brain stem reduces the enhanced sympathetic drive in mice with HF. Myocardial infarction (MI) was induced in mice by ligating the left coronary artery. MI mice exhibited left ventricular dilatation and a reduced left ventricular ejection fraction. Urinary norepinephrine excretion in MI mice was greater than that in sham-operated mice, indicating that sympathetic drive was enhanced in this model. Thus this model has features that are typical of HF. Western blot analysis and immunohistochemical staining for neuronal NOS (nNOS) indicated that nNOS protein expression was significantly reduced in the brain stem of MI mice. MI mice had a significantly smaller increase in blood pressure evoked by intracisternal injection of N^G-monomethyl-L-arginine than sham-operated mice. Adenoviral vectors encoding either eNOS (AdeNOS) or β-galactosidase (Adβgal) were transfected into the NTS to examine the effect of increased NO production in the NTS on the enhanced sympathetic drive in HF. After the gene transfer, urinary norepinephrine excretion was reduced in AdeNOS-transfected MI mice but not in Adβgal-transfected MI mice. These results indicate that nNOS expression in the brain stem, especially in the NTS, is reduced in the MI mouse model of HF, and increased NO production induced by overexpression of eNOS in the NTS attenuates the enhanced sympathetic drive in this model.

nitric oxide; heart failure; brain; sympathetic; genes

CHRONIC HEART FAILURE (HF) is characterized by enhanced neurohumoral drive in experimental animals as well as in patients (27, 29, 55). Sympathetic and humoral activation precede the onset of clinically recognized HF (11). In particular, there is accumulating evidence that β-blockers are one of the most effective drugs for treatment of patients with chronic HF (3, 31, 48), supporting the idea that the activation of the sympathetic nervous system has an important role in the progression of HF. In fact, plasma norepinephrine levels increase in relation to the severity of HF and correlate with mortality rates in patients with chronic HF (4, 38). The exact mechanisms underlying sympathoexcitation in HF are not clear, although several mechanisms have been proposed. Recent studies (27, 29, 55) suggest that the central nervous system (CNS) is involved in the mechanism(s) underlying sympathoexcitation in HF.

The nucleus tractus solitarius (NTS) in the brain stem is involved in regulating blood pressure, heart rate, and sympathetic nerve activity (1, 5, 23). The NTS receives inputs from afferent fibers arising from arterial baroreceptors, chemoreceptors, cardiopulmonary receptors, and other visceral receptors and thus has an important role in autonomic control of the cardiovascular system (1, 5, 23). There is considerable evidence that nitric oxide (NO) in the CNS, including the NTS, inhibits sympathetic nerve activity (14, 16, 33, 46, 52). In addition, there are high concentrations of neuronal NO synthase (nNOS) in brain stem regions, particularly in the NTS, as demonstrated by immunohistochemistry, NADPH-diaphorase staining, and autoradiography studies (7, 13, 47). Recent studies (18, 33, 50, 54) demonstrated reduced nNOS expression in the paraventricular nucleus (PVN) of the hypothalamus in a rat model of HF. Although the mRNA level of nNOS in the brain stem is reduced (33), the pathophysiological role of NO in the brain stem, particularly in the NTS, in HF is not known. Thus a more precise physiological investigation related to the NTS is necessary.

Therefore, we hypothesized that NOS in the brain stem, particularly in the NTS, is altered in HF, and this alteration contributes to the sympathoexcitation in the mouse model with HF. The aim of the present study was to determine whether endogenous nNOS in the brain stem is reduced in a mouse model of HF. Myocardial infarction (MI) was produced by left coronary artery (LCA) occlusion in mice to determine whether this model exhibits sympathoexcitation similar to that in human HF and changes in nNOS expression. Second, we transfected adenoviral vectors encoding endothelial NOS (AdeNOS) into the NTS to increase local NO production in the NTS of mice, using a technique previously established in rats (17, 22, 39). Urinary norepinephrine excretion was measured as a marker of the sympathetic nerve activity. We examined the effect of increased NO production induced by the transfection of AdeNOS in the NTS on sympathetic nerve activity.

METHODS

Animals and surgery. This study was reviewed and approved by the Committee on Ethics of Animal Experiments, Faculty of Medicine, Kyushu University, and conducted according to the *Guidelines for Animal Experiments of the Faculty of Medicine*, Kyushu University (Fukuoka, Japan). Male CD-1 mice (10 to 12 wk old, weight 30–40 g, Charles River Japan, Yokohama, Japan) underwent coronary artery

Address for reprint requests and other correspondence: Y. Hirooka, Dept. of Cardiovascular Medicine, Kyushu Univ. Graduate School of Medical Sciences, 3-1-1 Maidashi, Higashi-ku, Fukuoka 812-8582, Japan (e-mail: hyoshi@cardiol.med.kyushu-u.ac.jp).

The costs of publication of this article were defrayed in part by the payment of page charges. The article must therefore be hereby marked "*advertisement*" in accordance with 18 U.S.C. Section 1734 solely to indicate this fact.